Landau-Ginzburg theory of cortex dynamics: scale-free avalanches emerge at the edge of synchronization

Serena di Santo[a,b,c,1], **Pablo Villegas**[a,1], **Raffaella Burioni**[b,c], **and Miguel A. Muñoz**[a,2]

[a]Departamento de Electromagnetismo y Física de la Materia e Instituto Carlos I de Física Teórica y Computacional. Universidad de Granada. E-18071, Granada, Spain; [b]Dipartimento di Fisica e Scienza della Terra, Università di Parma, via G.P. Usberti, 7/A - 43124, Parma, Italy; [c]INFN, Gruppo Collegato di Parma, via G.P. Usberti, 7/A - 43124, Parma, Italy

This manuscript was compiled on November 21, 2021

arXiv:1801.10356v1 [q-bio.NC] 31 Jan 2018

Understanding the origin, nature and functional significance of complex patterns of neural activity, as recorded by diverse electrophysiological and neuroimaging techniques, is a central challenge in Neuroscience. Such patterns include collective oscillations, emerging out of neural synchronization, as well as highly-heterogeneous outbursts of activity interspersed by periods of quiescence, called "neuronal avalanches". Much debate has been generated about the possible scale-invariance or criticality of such avalanches, and its relevance for brain function. Aimed at shedding light onto this, here we analyze the large-scale collective properties of the cortex by using a mesoscopic approach, following the principle of parsimony of Landau-Ginzburg. Our model is similar to that of Wilson-Cowan for neural dynamics but, crucially, including stochasticity and space; synaptic plasticity and inhibition are considered as possible regulatory mechanisms. Detailed analyses uncover a phase diagram including down-states, synchronous, asynchronous, and up-state phases, and reveal that empirical findings for neuronal avalanches are consistently reproduced by tuning our model to the edge of synchronization. This reveals that the putative criticality of cortical dynamics does not correspond to a quiescent-to-active phase transition, as usually assumed in theoretical approaches, but to a synchronization phase transition, at which incipient oscillations and scale-free avalanches coexist. Furthermore, our model also accounts for up and down states as they occur, e.g. during deep sleep. The present approach constitutes a framework to rationalize the possible collective phases and phase transitions of cortical networks in simple terms, thus helping shed light into basic aspects of brain functioning from a very broad perspective.

Cortical dynamics | Neuronal avalanches | Criticality | Synaptic plasticity

The cerebral cortex exhibits spontaneous activity even in the absence of any task or external stimuli (1–3). A salient aspect of this, so-called, *resting-state* dynamics, as revealed by *in vivo* and *in vitro* measurements, is that it exhibits outbursts of electrochemical activity, characterized by brief episodes of coherence –during which many neurons fire within a narrow time window– interspaced by periods of relative quiescence, giving rise to collective oscillatory rhythms (4, 5). Shedding light on the origin, nature, and functional meaning of such an intricate dynamics is a fundamental challenge in Neuroscience (6).

Upon experimentally enhancing the spatio-temporal resolution of activity recordings, Beggs and Plenz made the remarkable finding that, actually, synchronized outbursts of neural activity could be decomposed into complex spatio-temporal patterns, thereon named "neuronal avalanches" (7). The sizes and durations of such avalanches were reported to be distributed as power-laws, i.e. to be organized in a scale-free way, limited only by network size (7). Furthermore, they obey finite-size scaling (8), a trademark of scale invariance (9), and the corresponding exponents are compatible with those of an unbiased branching process (10).

Scale-free avalanches of neuronal activity have been consistently reported to occur across neural tissues, preparation types, experimental techniques, scales, and species (11–18). This has been taken as empirical evidence backing the criticality hypothesis, i.e. the conjecture that the awake brain might extract essential functional advantages –including maximal sensitivity to stimuli, large dynamical repertoires, optimal computational capabilities, etc.– from operating close to a critical point, separating two different phases (19–22).

In order to make further progress, it is of crucial importance to clarify the nature of the phase transition marked by such an alleged critical point. It is usually assumed that it corresponds to the threshold at which neural activity propagates marginally in the network, i.e. to the critical point of a quiescent-to-active phase transition (7), justifying the emergence of branching-process exponents (23, 24). However, several experimental investigations found evidence that scale-free avalanches emerge in concomitance with collective oscillations, suggesting the

Significance Statement

The human cortex operates in a state of restless activity, whose meaning and functionality are still not well understood. A fascinating though still controversial hypothesis, to some extent backed by empirical evidence, suggests that the cortex might work at the edge of a phase transition, from which important functional advantages stem. However, the nature of such a phase transition is still not fully understood. Here, we adopt ideas from the physics of phase transitions, to construct a general (Landau-Ginzburg) theory of cortical networks, allowing us to analyze their possible collective phases and phase transitions. We conclude that the empirically reported scale-invariant avalanches can possibly come about if the cortex operated at the edge of a synchronization phase transition, at which neuronal avalanches and incipient oscillations coexist.

All authors designed the project, analyzed data, and wrote the paper; S. d. S. and P. V. performed the computational analyses.

The authors declare no conflict of interest.

[1]S.d.S and P.V. contributed equally to this work.

[2]To whom correspondence should be addressed. E-mail: mamunoz@onsager.ugr.es

presence of a synchronization phase transition (25, 26).

From the theoretical side, on the one hand, very interesting models accounting for the self-organization of neural networks to the neighborhood of the critical point of a quiescent-to-active phase transition have been proposed (27–30). These approaches rely on diverse regulatory mechanisms (31), such as synaptic plasticity (32), spike-time-dependent plasticity (33), excitability adaptation, etc. to achieve network self-organization to the vicinity of a critical point. These models have in common that they rely on an extremely large separation of dynamical timescales (as in models of self-organized criticality* (36, 37)) which might not be a realistic assumption (27, 30, 38, 39). Some other models are more realistic from a neurophysiological viewpoint (17, 29), but they give rise to scale-free avalanches if and only if causal information –which is available in computational models but not accessible in experiments (40)– is considered. Thus, in our opinion, a sound theoretical model justifying the empirical observation of putative criticality is still missing.

On the other hand, from the synchronization viewpoint, well-known simple models of networks of excitatory and inhibitory spiking neurons exhibit differentiated synchronous (oscillatory) and asynchronous phases, with a synchronization phase transition in between (41–44). However, avalanches do not usually appear (or are not searched for) in such modeling approaches (see, however, (18, 45, 46)).

Concurrently, during deep sleep and also under anesthesia the cortical state has long been known to exhibit, so called, "up and down" transitions between states of high and low neural activity, respectively (47, 48), which clearly deviate from the possible criticality of the awake brain, and which have been modeled on their own (29, 49, 50). Thus, it would be highly desirable to design theoretical models describing within a common framework the possibility of criticality, oscillations, and up-down transitions.

Our aim here is to clarify the nature of the phases and phase transitions of dynamical network models of the cortex by constructing a general unifying theory based on minimal assumptions and allowing us, in particular, to elucidate what the nature of the alleged criticality is.

To construct such a theory we follow the strategy pioneered by Landau and Ginzburg. Landau proposed a simple approach to the analysis of phases of matter and the phase transitions they experience. It consists in a parsimonious, coarse-grained, and deterministic description of states of matter in which –relying on the idea of universality– only relevant ingredients (such as symmetries and conservation laws) need to be taken into account and in which most microscopic details are safely neglected (9, 51). Ginzburg went a step further by realizing that fluctuations are an essential ingredient to be included in any sound theory of phase transitions, especially in low-dimensional systems. The resulting Landau-Ginzburg theory, including fluctuations and spatial dependence is regarded as a *meta-model* of phase transitions and constitutes a firm ground on top of which the standard theory of phases of matter rests (9). Similar coarse-grained theories are nowadays used in interdisciplinary contexts – such as collective motion (52), population dynamics (53), and neuroscience (54–56)– where diverse collective phases stem out of the interactions among many elementary constituents.

In what follows we propose and analyze a Landau-Ginzburg theory for cortical neural networks –which can be seen as a variant of the well-known Wilson-Cowan model including, crucially, stochasticity and spatial dependence– allowing us to shed light from a very general perspective on the collective phases and phase transitions that dynamical cortical networks can harbor. Employing analytical and, mostly, computational techniques, we show that our theory explains the emergence of scale-free avalanches, as episodes of marginal and transient synchronization in the presence of a background of ongoing irregular activity, reconciling the oscillatory behavior of cortical networks with the presence of scale-free avalanches. Last but not least, our approach also allows for a unification of existing models describing diverse specific aspects of the cortical dynamics, such as up and down states and up-and-down transitions, within a common mathematical framework, and is amenable of future theoretical (e.g. renormalization group) analyses.

Model and Results

We construct a mesoscopic description of neuronal activity, where the building blocks are not single neurons but local neural populations. These latter can be thought as small sections of neural tissue (57, 58) consisting of a few thousand cells (far away from the large-network limit), and susceptible to be described by a few variables. Even though this effective description is constructed here on phenomenological bases, more formal mathematical derivations of similar equations from microscopic models exist in the literature (see e.g. (59)). In what follows, first (i) we model the neural activity at a single mesoscopic "unit", then (ii) we analyze its deterministic behavior as a function of parameter values, and later on (iii) we study the collective dynamics of many coupled units.

Single-unit model. At each single unit we consider a dynamical model in which the excitatory activity, ρ, obeys a Wilson-Cowan equation (60) (that, following the Landau approach, we truncate to third order in a Taylor series expansion)†:

$$\dot{\rho}(t) = \big[-a + R(t) \big] \rho(t) + b\rho^2(t) - \rho^3(t) + h \qquad [1]$$

where $a > 0$ controls the spontaneous decay of activity, which is partially compensated by the generation of additional activity at a rate proportional to the amount of available *synaptic resources*, $R(t)$; the quadratic term with $b > 0$, controls non-linear integration effects‡; finally, the cubic term imposes a saturation level for the activity, preventing unbounded growth, and h is an external driving field.

A second equation is employed to describe the dynamics of the available synaptic resources, $R(t)$, through the combined effect of synaptic depression and synaptic recovery, as encoded in the celebrated model of Tsodyks and Markram (TM) for synaptic plasticity (32, 61):

$$\dot{R}(t) = \frac{1}{\tau_R}(\xi - R(t)) - \frac{1}{\tau_D} R(t)\rho(t), \qquad [2]$$

*This theory, developed three decades ago aims at explaining the seemingly ubiquitous presence of criticality in natural systems as the result of auto-organization to the critical point of a quiescent/active phase transition by means of diverse mechanisms, including the presence of two dynamical processes occurring at infinitely separated timescales (34, 35).

†We keep up to third order to include the leading effects of the sigmoid response function; a non-truncated variant of the model has also been considered; see SI appendix SI1.

‡Single neurons integrate many presynaptic spikes to go beyond threshold, and thus their response is non-linear: the more activity the more likely it is self-sustained (57). As a matter of fact, the Wilson-Cowan model includes a sigmoid response function with a threshold, implying that activity has to be above some minimum value to be self-sustained, and entailing $b > 0$ in the series expansion (see Methods).

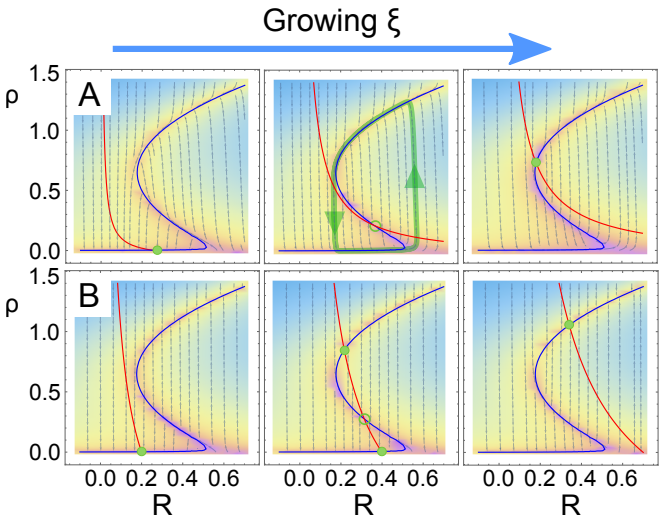


Fig. 1. Phase portraits and nullclines for the (deterministic) dynamics, Eqs.(1) and (2). Nullclines are colored in blue ($\dot{\rho} = 0$) and red ($\dot{R} = 0$), respectively; fixed points (ρ^*, R^*) –at which nullclines intersect– are highlighted by green full (empty) circles for stable (unstable) fixed points. Background color code (shifting from blue to purple) represents the intensity of the vector field $(\dot{\rho}, \dot{R})$, whose local directions are represented by small grey arrows. A trajectory illustrating a limit cycle is showed in green in (A). The system exhibits either (A) an oscillatory regime or (B) a region of bistability, in between a down (left) and an up (right) state. It is possible to shift from case (A) to case (B) and viceversa by changing just one parameter; e.g. the timescale of resources depletion, τ_D^{-1} (0.016 and 0.001 for cases (A) and (B), respectively). Other parameter values: $h = 10^{-3}, a = 0.6, b = 1.3, \tau_R = 10^3$; control parameter, from left to right, $\xi = 0.3, 1.6, 2.3$ in the upper panel and $\xi = 0.2, 0.4, 0.7$ in the lower one.

where τ_R (resp. τ_D) is the characteristic recovery (depletion) time, and ξ is the baseline level of non-depleted synaptic resources. Importantly, we have also considered variants of this model, avoiding the truncation of the power-series expansion, or including an inhibitory population as the chief regulatory mechanism: either of these extensions leads to essentially the same phenomenology and phases as described in what follows, supporting the robustness of the forthcoming results (see Supp. Appendix SI1).

Mean-field analysis. Here we analyze, both analytically and computationally, the dynamics of a single unit, as given by Eqs.(1) and (2). First, we determine the fixed points (ρ^*, R^*) –i.e. the possible steady-states at which the system can settle– as a function of the baseline-level of synaptic resources, ξ, which plays the role of a control parameter (all other parameters are kept fixed to standard non-specific values, as summarized in the caption of Fig.1). For small values of ξ, the system falls into a quiescent or *down* state with $\rho^* \approx 0$ and $R^* \approx \xi$[§]. Instead, for large values of ξ there is an active or *up* state with self-sustained spontaneous activity $\rho^* > 0$ and depleted resources $R^* < \xi$. In between these two limiting phases, two alternative scenarios (as illustrated in Fig.1 and summarized in the phase diagram of Suppl. Inf. SI2) can appear depending on the time scales τ_D and τ_R:

(A) A stable limit cycle (corresponding to an unstable fixed point with complex eigenvalues) emerges for intermediate values of ξ (in between two Hopf bifurcations) as illustrated in Fig.1A. This Hopf-bifurcation scenario has been extensively discussed in the literature (see e.g. (62)) and it is at the basis of the emergence of oscillations in neural circuits.

(B) An intermediate regime of bistability including three fixed points is found for intermediate values of ξ (in between two saddle-node bifurcations): the up and the down ones, as well as an unstable fixed point in between (as illustrated in Fig.1B). This saddle-node scenario is the relevant one in models describing transitions between up (active) and down (quiescent) states (29, 49, 63).

Two remarks are in order. The first is that one can shift from one scenario to the other just by changing one parameter, e.g. the synaptic depletion timescale τ_D[¶]. The second and very important one is that none of these two scenarios exhibits a continuous transition (transcritical bifurcation) separating the up/active from the down/quiescent regimes. Thus, at this single-unit/deterministic level, there is no precursor of a critical point for marginal propagation of activity.

Stochastic network model. We now introduce stochastic and spatial effects in the simplest possible way. For this, we consider a network of N nodes coupled following a given connection pattern, as described below. Each network node represents a mesoscopic region of neural tissue or "unit" as described above. On top of this deterministic dynamics, we consider that each unit (describing a finite population) is affected by intrinsic fluctuations (55, 59, 64). More specifically, Eq.(1) is complemented with an additional term $+A(\rho)\eta(t)$ which includes a (zero-mean, unit-variance) Gaussian noise $\eta(t)$ and a density-dependent amplitude $A(\rho)$[‖] i.e. a multiplicative noise (65).

At macroscopic scales, the cortex can be treated as a two-dimensional sheet consisting mostly of short-range connections (66)[**]. Although long-range connections are also known to exist, and small-world effects have been identified in local cortical regions (68), here we consider a two-dimensional square lattice (size $N = L^2$) of mesoscopic units as the simplest way to embed our model into space. Afterward, we shall explore how our main results are affected by the introduction of more realistic network architectures including additional layers of complexity such as long-range connections and spatial heterogeneity.

Following the parsimonious Landau-Ginzburg approach adopted here, the coupling between neighboring units is described up to leading order by a diffusion term. This type of diffusive coupling between neighboring mesoscopic units stems from electrical synapses (57, 69), has some experimental backing (70), and has been analytically derived starting from models of spiking neurons (54) [††]. Thus, finally, the resulting

[§] Deviations from $\rho^* = 0$ stem from the small but non-vanishing external driving $h \neq 0$.

[¶] Note that the slope of the nullcline deriving from Eq.(2) (red in Fig.1) is proportional to τ_D: if it is small enough, there exists only one unstable fixed point, giving rise to a Hopf bifurcation; otherwise the nullclines intersect at three points, generating the bistable regime. These two possibilities correspond to cases A and B above, respectively.

[‖] In the limit of slow external driving and up to leading order in an expansion in powers of ρ, this can be written as $A(\rho) = \sigma\sqrt{\rho(t)}$, where σ is a noise amplitude; this stems from the fact that the spiking of each single neuron is a stochastic process, and the overall fluctuation of the density of a collection of them scales with its square-root, as dictated by the central limit theorem (65) (see also (59) for a detailed derivation of the square-root dependence).

[**] This type of approach is at the bases of, so-called, neural-field models, with a long tradition in neuroscience (67).

[††] More elaborated approaches including coupling kernels between different regions, as well as asymmetric ones, are also often considered in the literature (e.g. (56)), but here we stick to the simplest possible coupling.

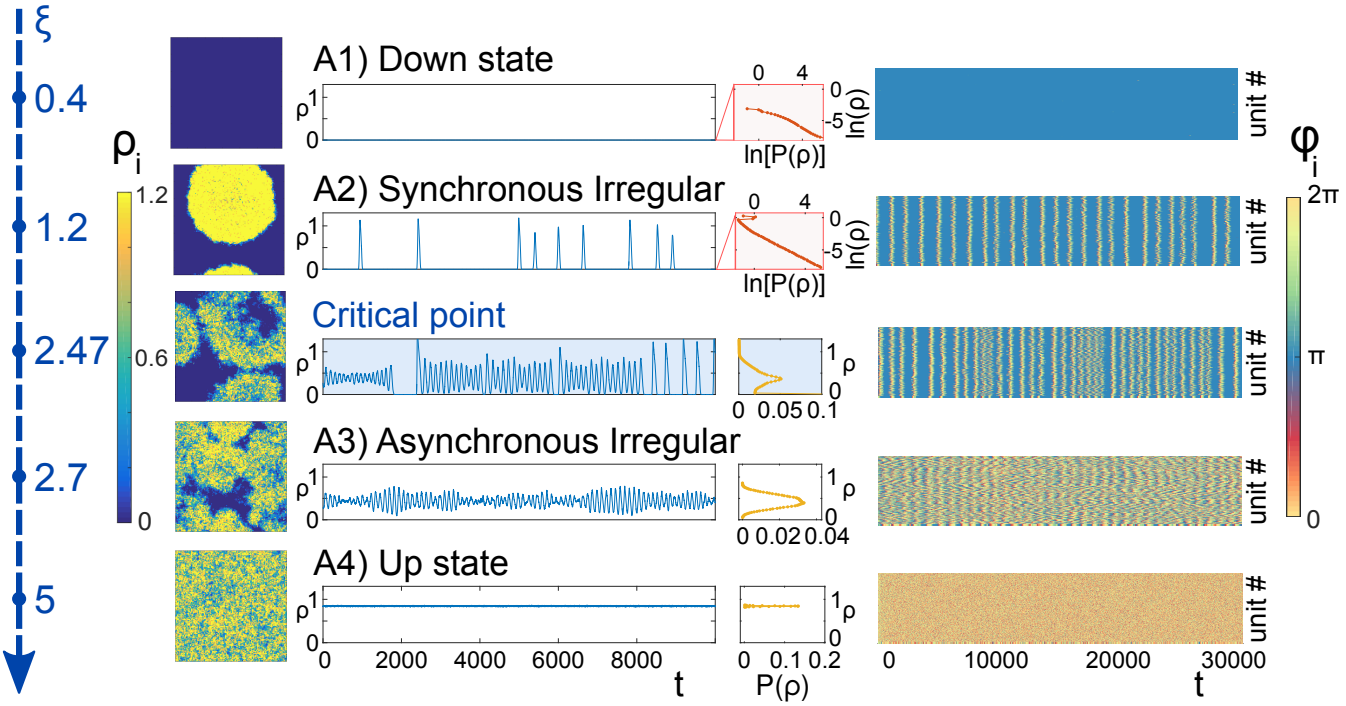


Fig. 2. Illustration of the diverse phases emerging in the model (case A). The baseline of synaptic resources, ξ, increases from top to bottom: $\xi = 0.4$ (down-state), $\xi = 1.2$ (synchronous regime), $\xi = 2.47$ (critical point for the considered size, $N = 128^2$), $\xi = 2.7$ (asynchronous phase), and $\xi = 5$ (active phase). *First column:* Snapshots of typical configurations; the color code represents the level of activity at each unit as shown in the scale. The network-spiking or synchronous irregular phase, is characterized by waves of activity growing and transiently invading the whole system, before extinguishing the resources and coming to an end. On the other hand, in the nested-oscillation or asynchronous irregular regime multiple traveling waves coexist, interfering with each other. In the up-state waves are no longer observed and a homogeneous state of self-sustained activity is observed (see also the videos in SI-Movie). *Second column:* Time series of the overall activity averaged over the whole network. In the down state activity is almost vanishing. In the synchronous phase macroscopic activity appears in the form of almost synchronous bursts, interspersed by almost silent intervals. At the critical point network spikes begin to superimpose, giving rise to complex oscillatory patterns (nested oscillations) and marginally self-sustained global activity all across the asynchronous regime; finally, in the up state the global activity converges to steady-state with small fluctuations. *Third column:* Steady state probability distribution $P(\rho)$ for the global activity: in the down state and the network spiking regime the distributions are shown in a double-logarithmic scale; observe the approximate power-law for very small values of ρ stemming from the presence of multiplicative noise (10). *Fourth column:* Illustration of the different levels of synchronization across phases: a sample of 200 randomly chosen units are mapped into oscillators using their *analytic-signal representation* (see Methods); the plot shows the time evolution of their corresponding phases ϕ_k^A. Observe the almost periodic behavior in the synchronous phase, which starts blurring at the critical point, and progressively vanishes as the control parameter is further increased. Parameter values: $a = 1, b = 1.5, \tau_R = 10^3, \tau_D = 10^2, h = 10^{-7}$.

set of coupled stochastic equations is:

$$\begin{cases} \dot{\rho}_i(t) = (-a + R_i)\rho_i + b\rho_i^2 - \rho_i^3 + h + D\nabla^2\rho_i + \sigma\sqrt{\rho_i}\eta_i \\ \dot{R}_i(t) = \frac{1}{\tau_R}(\xi - R_i) - \frac{1}{\tau_D}R_i\rho_i \end{cases} \quad [3]$$

where, for simplicity, some time dependences have been omitted; $\rho_i(t)$ and $R_i(t)$ are, respectively, the activity and resources at a given node i (with $i = 1, 2, ...N$) and time t, $D\nabla^2\rho_i \equiv D\sum_{j\in n.n.i}(\rho_j - \rho_i)$, describes the diffusive coupling of unit i with its nearest neighbors j, with (diffusion) constant D. The physical scales of the system are controlled by the values of the parameters D and σ; however, given that, as illustrated in SI2, results do not change qualitatively upon varying parameter values (as long as they are finite and non-vanishing), here we take $D = \sigma = 1$ for the sake of simplicity.

Eq.(3) constitutes the basis of our theory. In principle, this set of equations is amenable to theoretical analyses, possibly including renormalization ones (9). However, here we restrict ourselves to computational studies aimed at scrutinizing what is the basic phenomenology, leaving more formal analyses for the future. In particular, we resort to numerical integration of the stochastic equations Eq.3, which is feasible thanks to the efficient scheme developed in (71) to deal with multiplicative noise. We consider $\delta t = 0.01$ as an integration timestep and keep, as above, all parameters fixed, except for the baseline level of synaptic resources, ξ, which works as a control parameter.

Phases and phase transitions: Case A. We start analyzing a sets of parameters lying within case A above. We study the possible phases that emerge as ξ is varied. These are illustrated in Fig. 2 where characteristic snapshots, overall-activity time series, as well as raster plots are plotted. For a more vivid visualization, we have also generated videos of the activity dynamics in the different phases (see SI-Movie).

A1) Down-state phase. If the baseline level ξ is sufficiently small ($\xi \lesssim 0.75$), resources R are always scarce and the system is unable to produce self-sustained activity (i.e. it is hardly excitable) giving rise to a down-state phase, characterized by very small values of the network time-averaged activity $\bar{\rho} \equiv \frac{1}{T}\int_0^T dt \frac{1}{N}\sum_{i=1}^N \rho_i(t)$ for large times T (see Fig.2 first row). The quiescent state is disrupted only locally by the effect of the driving field h, which creates local activity, barely propagating to neighboring units.

A2) Synchronous irregular (SI) phase. Above a certain value of resource baseline ($\xi \gtrsim 0.75$) there exists a wide region in parameter space in which activity generated at a seed point is able to propagate to neighboring units, triggering a wave of activity which transiently propagates through the network until resources are exhausted, activity ceases, and the recovery process restarts (see Fig. 2 second row). Such waves or "network-spikes" appear in an oscillatory, though not perfectly periodic, fashion, with an average separation time that decreases with ξ. In the terminology of Brunel (43), this corresponds to a *synchronous irregular* (SI) state/phase, since the collective activity is time-dependent (oscillatory) and single-unit spiking is irregular (as discussed below). This wax-and-wane dynamics resembles that of anomalous, e.g. epileptic, tissues (72).

A3) Asynchronous irregular (AI) phase. For even larger values of resource baseline ($\xi \gtrsim 2.15$), the level of synaptic recovery is sufficiently high as to allow for resource-depleted regions to recover before the previous wave has come to an end. Thereby, diverse travelling waves can coexist and interfere, giving rise to complex collective oscillatory patterns (see Fig. 2 fourth row, which is strikingly similar to, e.g. EEG data of $\alpha-$rhythms (73)). The amplitude of these oscillations, however, decreases upon increasing network size (which occurs as many different local waves are averaged and deviations from the mean tend to be washed away). This regime can be assimilated to an *asynchronous irregular* (AI) phase of Brunel (43) (see below).

A4) Up-state phase. For even larger values of ξ, plenty of synaptic resources are available at all times, giving rise to a state of perpetual activity with small fluctuations around the mean value (Fig. 2 fifth row), i.e. an up state. Let us finally remark, that as explicitly shown in the SI5, the AI phase and the Up-state cannot be distinguished in the infinite network-size limit, in which there are so many waves to be averaged that a homogeneous steady state emerges on average in both cases.

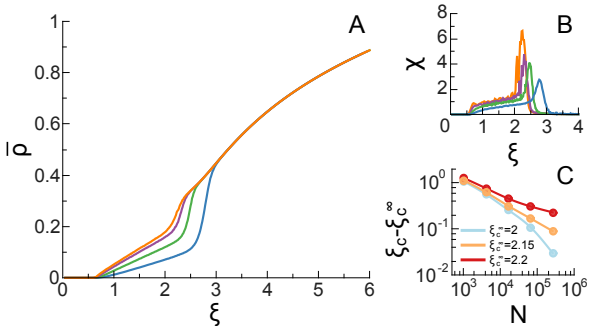


Fig. 3. Overall network activity state (case A) as determined by the network time-averaged value $\bar{\rho}$ ($h = 10^{-7}$). (A) Order parameter $\bar{\rho}$ as a function of the control parameter ξ for various system sizes $N = 64^2, 128^2, 256^2, 512^2$ (from bottom (blue) to top (orange)); observe that $\bar{\rho}$ grows monotonically with ξ and that an intermediate regime, in which $\bar{\rho}$ grows with system size, emerges between the up and the down states. (B) Standard deviation of the averaged overall activity in the system multiplied by $\sqrt{N}$; $\Xi = \sigma_\rho \sqrt{N}$ (see main text); The point of maximal variability coincides with the point of maximal slope in (A) for all network sizes N. (C) Finite-size scaling analysis of the peaks in (B). The distance of the size-dependent peak locations $\xi_c(N)$ from their asymptotic value for $N \to \infty$, ξ_c^∞, scales as a power law of the system size, taking $\xi_c^\infty \approx 2.15$, revealing the existence of true scaling at criticality.

Phase transitions. Having analyzed the possible phases, we now discuss the phase transitions separating them. For all the considered network sizes the time-averaged overall activity, $\bar{\rho}$, starts taking a distinctively non-zero value above $\xi \approx 0.75$ (see Fig.3), reflecting the upper bound of the down or quiescent state (transition between A1 and A2). This phase transition is rather trivial and corresponds to the onset on network spikes i.e. oscillations (whose characteristic time depends on various factors, such as the synaptic recovery time (74) and the baseline level of synaptic resources).

More interestingly, Fig.3 also reveals that $\bar{\rho}$ exhibits an abrupt increase at (size-dependent) values of ξ, between 2 and 3, signaling the transition from A2 to A3. However, the jump amplitude decreases as N increases, suggesting a smoother transition in the large-N limit. Thus it is not clear *a priori*, using $\bar{\rho}$ as an order parameter, whether there is a true sharp phase transition or there is just a crossover between the synchronous (A2) and the asynchronous (A3) regimes. To elucidate the existence of a true critical point, we measured the standard deviation of the network-averaged global activity $\bar{\rho}$, σ_ρ. Direct application of the central limit theorem (65) would imply that such a quantity should decrease as $1/\sqrt{N}$ for large N and thus, $\chi \equiv \sqrt{N}\sigma_\rho$ should converge to a constant. However, Fig. 3B shows that χ exhibits a very pronounced peak located at the (N-dependent) transition point between the A2 and the A3 phases; furthermore its height grows with N –i.e. it diverges in the thermodynamic limit– revealing strong correlations and anomalous scaling, as occurs at critical points. Also, a finite-size scaling analysis of the value of ξ at the peak (for each N), i.e. $\xi_c(N)$, reveals the existence of finite-size scaling, as corresponds to a *bona fide* continuous phase transition at $\xi_c^\infty \simeq 2.15(5)$ in the infinite-size limit (see Fig. 3C). Moreover, a detrended fluctuation analysis (75, 76) of the timeseries reveals the emergence of long-range temporal correlations right at ξ_c (see SI4), as expected at a continuous phase transition.

To shed further light on the nature of such a transition, it is convenient to employ a more adequate (synchronization) order-parameter. In particular, we consider the Kuramoto index K –customarily employed to detect synchronization transitions (77)– defined as $K \equiv \frac{1}{N}\left\langle \left| \sum_{k=1}^{N} e^{i\phi_k(t)} \right| \right\rangle$ –where i is the imaginary unit, $|\cdot|$ is the modulus of a complex number, $\langle\cdot\rangle$ here indicates averages over time and independent realizations, and k runs over units, each of which is characterized by a phase, $\phi_k(t) \in [0, 2\pi]$, that can be defined in different ways. For instance, an effective phase $\phi_k^{\mathcal{A}}(t)$ can be assigned to the time-series at unit k, $\rho_k(t)$, by computing its *analytic signal representation*, which maps any given real-valued timeseries into an oscillator with time-dependent phase and amplitude (see Methods). Using the resulting phases, $\phi_k^{\mathcal{A}}(t)$, the Kuramoto index $K_{\mathcal{A}}$ can be calculated. As illustrated in Fig. 4A, it reveals the presence of a synchronization transition: the value of $K_{\mathcal{A}}$ clearly drops, at the previously determined critical point $\xi_c(N)$. An alternative method to define a time-dependent phase for each unit (details discussed in Methods) reveals even more vividly the existence of a synchronization transition at $\xi_c(N)$ as shown in Fig. 4B. Finally, we have also estimated the coefficient of variation (CV) of the distance between the times at which each of these effective phases crosses the value 2π; this analysis reveals the presence of a sharp peak of variability, converging for large network sizes to the critical point $\xi_c^\infty \approx 2.15$ (see inset of Fig. 4B).

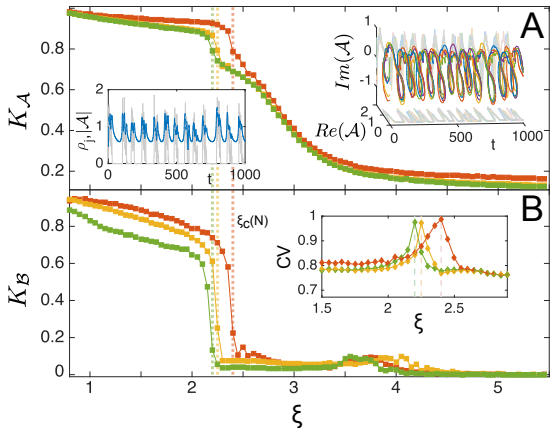


Fig. 4. Synchronization transition elucidated by measuring the Kuramoto parameter as estimated using (A) the analytic signal representation $\mathcal{A}_k(t)$ of activity time series $\rho_k(t)$ at different units k and for various system sizes ($N = 128^2$ (red), 256^2 (orange), 512^2 (green)). For illustrative purposes, the top right inset of (A) shows the analytical representation (including both a real and an imaginary part) of 5 sample units as a function of time; the inset on the left shows the time evolution of one node (gray) together with the amplitude of its analytic representation (blue) Both insets, vividly illustrate the oscillatory nature of the unit dynamics. (B) Results similar to those of (A), but employing a different method to compute time-dependent phases of effective oscillators (see Methods). This alternative method captures more clearly the emergence of a transition; the point of maximum slope of the curves corresponds to the value of the transition points $\xi_c(N)$ in (A). The inset in (B) shows the coefficient of variation CV (ratio of the standard deviation to the mean) of the times between two consecutive crossings of the value 2π; it exhibits a peak of variability at the critical point $\xi_c(N)$.

Thus, recapitulating, the phase transition separating the down state from the synchronous irregular regime (A1-A2 transition) is trivial and corresponds to the onset of network spikes, with no sign of critical features. In between the asynchronous and the up state (A3-A4) there is no true phase transition, as both phases are indistinguishable in the infinitely-large-size limit (see SI5). On the other hand, different measurements clearly reveal the existence of a bona fide synchronization phase transition (A2-A3) at which non-trivial features characteristic of criticality emerge.

Avalanches. For ease of comparison with empirical results, we define a protocol to analyze avalanches that closely resembles the experimental one, as introduced by Beggs and Plenz (7). Each activity timeseries of an individual unit can be mapped into a series of discrete-time "spikes" or "events" as follows. As illustrated in Fig.5A, a "spike" corresponds to a period in which the activity at a given unit is above a given small threshold in between two windows of quiescence (activity below threshold).[‡‡] Hence, as illustrated in Fig.5B, the network activity can be represented as a raster plot of spiking units. Following the standard experimental protocol a discrete time binning Δt is chosen and each individual spike is assigned to one such bin. An avalanche is defined as a consecutive sequence of temporally-contiguous occupied bins preceded and ended by empty bins (see Fig.5B and C). Quite remarkably, using this protocol several well-known experimental key features of neuronal avalanches can be faithfully reproduced by tuning ξ to a value close to the synchronization transition. In particular:

[‡‡] Results are quite robust to the specific way in which this procedure is implemented. See the Methods section as well as the caption of Fig.5 and Supp. Inf. SI6).

(i) The sizes and durations of avalanches of activity are found to be broadly (power-law) distributed at the critical point; these scale-invariant avalanches coexist with anomalously large events or "waves" of synchronization, as revealed by the "heaps" in the tails of the curves of in Fig.5D and E.

(ii) Changing Δt, power-law distributions with varying exponents are obtained at criticality (the larger the time bin, the smaller the exponent) as originally observed experimentally by Beggs and Plenz (Fig.5E).

(iii) In particular, when Δt is chosen to be equal to the ISI (inter-spike time interval, i.e. the time interval between any two consecutive spikes), avalanche sizes and durations obey –at criticality– finite-size scaling with exponent values compatible with the standard ones, i.e. those of an unbiased branching process (see Fig.5B and C as well as Supporting Information SI6).

(iv) Reshuffling the times of occurrence of unit's spikes, the statistics of avalanches is dramatically changed, giving rise to exponential distributions (as expected for an uncorrelated Poisson point process) thus revealing the existence of a non-trivial temporal organization in the dynamics (Fig.5E).

(v) Away from the critical point, both in the sub-critical and in the supercritical regime, deviations from this behavior are observed; in the subcritical or synchronous regime, the peak of periodic large avalanches becomes much more pronounced, while in the asynchronous phase, such a peak is lost and distribution functions become exponential ones with a characteristic scale (see Fig.5D).

Summing up, our model tuned to the edge of a synchronization/desynchronization phase transition reproduces all chief empirical findings for neural avalanches. These findings strongly suggest that the critical point alluded by the criticality hypothesis of cortical dynamics does not correspond to a quiescent/active phase transition –as modeling approaches usually assume– but to a synchronization phase transition, at the edge of which oscillations and avalanches coexist.

It is important to underline that our results regarding the emergence of scale-free avalanches are purely computational. To date, we do not have a theoretical understanding of why results are compatible with branching-process exponents. In particular, it is not clear to us if a branching process could possibly emerge as an effective description of the actual (synchronization) dynamics in the vicinity of the phase transition, or whether the exponent values appear as a generic consequence of the way temporally-defined avalanches are measured (see (46)). These issues deserve to be carefully scrutinized in future work.

The role of heterogeneity. Thus far we have described homogeneous networks with local coupling. However, long-range connections among local regions also exist in the cortex, and mesoscopic units are not necessarily homogeneous across space (68, 78). These empirical facts motivated us to perform additional analysis of our theory, in which slightly modified substrates are employed. First, we considered small-world networks, and verified that our main results (i.e. the existing phases and phase transitions) are insensitive to the introduction of a small percentage of long-range connections (see SI3). However, details such as the boundaries of the phase diagram, the shape of propagation waves, and the amplitude of nested oscillations do change.

More remarkably, as described in detail in SI3, a simple

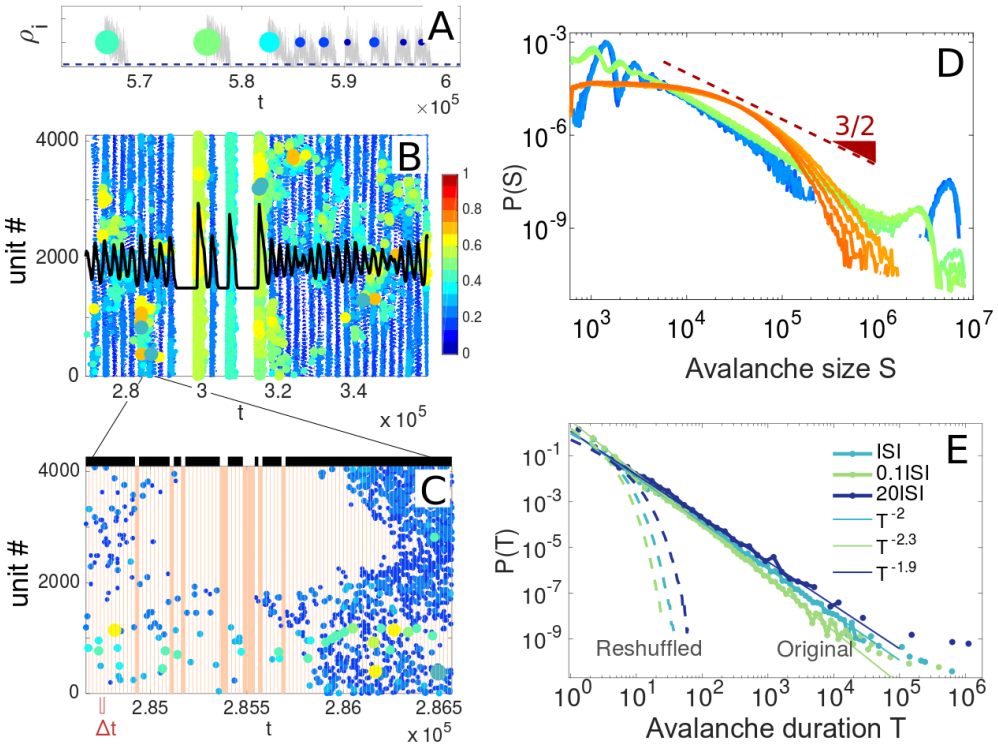


Fig. 5. Avalanches measured from activity time series. (A) Illustration of the activity timeseries $\rho_i(t)$ (grey color) at a given unit i. By establishing a threshold value θ (dashed blue line, close to the origin) a single "event" or "unit spike" is defined at the time of the maximal activity in between two threshold crossings (n.b. the forthcoming results are robust to changes in this criterion; see SI6); a weight equal to the area covered in between the two crossings is assigned to each event (note the color code). This allows us to map a continuous time-series into a discrete series of weighted events. The time distance between two consecutive events is called *inter-spike interval* (ISI). (B) Raster plot for a system with 64^2 units, obtained using the procedure above for each unit. Observe that large events coexist with smaller ones, and that these last ones, occur in a rather synchronous fashion. The overall time-dependent activity is marked with a black curve. (C) Zoom of a part of (B) illustrating the time resolved structure and using a time binning Δt equal to the network-averaged ISI. Shaded columns correspond to empty time bins, i.e. with no spike. Avalanches are defined as sequences of events occurring in between two consecutive empty time bins and are represented by the black bars above the plot. (D) Avalanche-size distribution (the size of the avalanche is the sum of the weighted spikes it comprises) for diverse values of ξ (from 1.85 to 2.05, in blueish colors, from 2.7 to 2.9 in greenish colors, and from 3.3 to 3.45 in orangish colors) measured from the raster plot $\Delta t = ISI$. The (red) triangle, with slope $3/2$ is plotted as a reference, illustrating that, near criticality, a power law with an exponent similar to the experimentally measured one is recovered. Away from the critical point, either in the synchronous phase (blueish colors) and the asynchronous one (orangish) clear deviations from power-law behavior are observed. Observe the presence of "heaps" in the tails of the distributions, especially in the synchronous regime; these correspond to periodic waves of synchronized activity (see SI7); they also appear at criticality, but at progressively larger values for larger system sizes. (E) Avalanche-duration distribution, determined with different choices of the time bin. The experimentally measured exponent ≈ 2 is reproduced using $\Delta t = ISI$, whereas deviations from such a value are measured for smaller (larger) time bins, in agreement with experimentally reported results. After reshuffling times, the distributions become exponential ones, with characteristic timescales depending on Δt (dashed lines).

extension of our theory in which parameters are not taken to be homogeneous but position-dependent, i.e. heterogeneous in space, is able to reproduce remarkably well empirical *in vitro* results for neural cultures with different levels of mesoscopic structural heterogeneity (79).

To further explore the influence of network architecture onto dynamical phases, in future work we will extend our model employing empirically-obtained large-scale networks of the human brain, as their heterogeneous and hierarchical-modular architecture is known to influence dynamical process operating on them (68, 80).

Phases and phase transitions: Case B. Here, we discuss the much simpler scenario for which the deterministic/mean-field dynamics predicts bistability, i.e. case B above, which is obtained e.g. considering a slower dynamic for synaptic-resource depletion. In this case, the introduction of noise and space, does not significantly alter the deterministic picture. Indeed, computational analyses reveal that there are only two phases: a down state and an up one for small and large values of ξ, respectively. These two phases have the very same features as their corresponding counterparts in case A. However, the phase transition between them is discontinuous (much as in Fig. 1B) and thus, for finite networks, fluctuations induce spontaneous transitions between the up and the down state when ξ takes intermediate values, in the regime of phase coexistence. Thus, in case B, our theory constitutes a sound Landau-Ginzburg description of existing models, such as those in (29, 49, 50), describing up and down states and up-and-down transitions.

Conclusions and Discussion

The brain of mammalians is in a state of perennial activity even in the absence of any apparent stimuli or task. Understanding the origin, meaning, and functional significance of such an energetically costly dynamical state are fundamental problems in neuroscience. The –so called– criticality hypothesis conjectures that the underlying dynamics of cortical networks is such that it is posed at the edge of a continuous phase transi-

tion, separating qualitatively different phases or regimes, with different degrees of order. Experience from statistical physics and the theory of phase transitions teaches that critical points are rather singular locations in phase diagrams, with very remarkable and peculiar features, such as scale invariance, i.e. the fact that fluctuations of wildly diverse spatio-temporal scales can emerge spontaneously, allowing the system dynamics to generate complex patterns of activity in a simple and natural way. A number of features of criticality, including scale invariance, have been conjectured to be functionally convenient and susceptible to be exploited by biological (as well as artificial) computing devices. Thus, the hypothesis that the brain actually works at the borderline of a phase transition has gained momentum in recent years (20–22), even if some skepticism remains (46). However, what these phases are, and what the nature of the putative critical point is, are questions that still remain to be fully settled.

Aimed at shedding light on these issues, here we followed a classical statistical-physics approach. Following the parsimony principle of Landau and Ginzburg in the study of phases of the matter and the phase transitions they experience, we proposed a simple stochastic mesoscopic theory of cortical dynamics that allowed us to classify the possible emerging phases of cortical networks under very general conditions. For the sake of specificity and concreteness we focused on a regulatory dynamics –preventing the level of activity to explode– controlled by synaptic plasticity (depletion and recovery of synaptic resources), but analogous results have been obtained considering e.g. inhibition as the chief regulatory mechanism. As a matter of fact, our main conclusions are quite robust and general and do not essentially depend on specific details of the implementation, the nature of the regulatory mechanism.

The mesoscopic approach upon which our theory rests is certainly not radically novel as quite a few related models exist in the literature. For instance, neural-mass (81–83) and neural-field models (66, 67), rate or population activity equations (58, 84), are similar in spirit, and have been successfully employed to analyze activity of populations of neurons and synapses, and their emerging collective regimes, at mesoscopic and macroscopic scales.

Taking advantage of experience from the theory of phase transitions, we introduce two important key ingredients: intrinsic stochasticity stemming from the non-infinite size of mesoscopic regions, and spatial dependence. In this way, our theory consists of a set of stochastic (truncated) Wilson-Cowan equations and can be formulated as a field theory, employing standard techniques (85). A rather similar (field theoretic) approach to analyze fluctuation effects in extended neural networks has been proposed (54).

Such a theory turns out to include a continuous phase transition from a quiescent to an active phase, with a critical point in between, which is in contrast with our findings here. Note, however, that the authors of (54) themselves open the door to more complex scenarios if refractoriness and thresholds are included.

In any case, such a continuous-phase-transition picture can be easily recovered in our framework, just by changing the sign of a parameter: i.e. taking $b < 0$ in Eq.(1); with such a parameter choice, our theory constitutes a sound Landau-Ginzburg description of microscopic models of neural dynamics exhibiting criticality and a continuous phase transition from a quiescent to an active phase (27, 39). We believe, however, that this scenario does not properly capture the essence of cortical dynamics as, in actual networks of spiking neurons, there are spike-integration mechanisms, meaning that many inputs are required to trigger further activity.

Using our Landau-Ginzburg approach, we have shown that the stochastic and spatially extended neural networks can harbor two different scenarios depending on parameter values: case (A) including a limit cycle at the deterministic level and the possibility of oscillations and case (B) leading to bistability (see Fig.1).

In the simpler case (B) our complete theory generates either a down or a homogeneous up-state phase, with a discontinuous transition separating them, and the possibility of up-down transitions when the system operates in the bistability region. In this case, our theory constitutes a sound mesoscopic description of existing microscopic models for up-and-down transitions (29, 49, 63, 86).

On the other hand, in case (A), we find diverse phases including oscillatory and bursting phenomena: down states, synchronous irregular, asynchronous irregular, and active states.

As a side remark, let us emphasize that we constructed a coarse-grained model for activity propagation, but our analyses readily revealed the emergence of oscillations and synchronization phenomena. Hence, our results justify the use of models of effective coupled oscillators to scrutinize the large-scale dynamics of brain networks. As a matter of fact, such models have been reported to achieve the best performance –e.g. reproducing empirically-observed resting-state networks (68)– when operating close to the synchronization phase transition point (64, 87, 88).

Within our framework, it is possible to define a protocol to analyze avalanches, resembling very closely the experimental one (7, 8, 11, 16, 17). Thus, in contrast with other computational models, causal information is not explicitly needed/employed here to determine avalanches –they are determined from raw data– and results can be straightforwardly compared to experimental ones for neuronal avalanches, without conceptual gaps (40).

The model reproduces all the main features observed experimentally: (i) Avalanche sizes and durations distributed in a scale-free way emerge at the critical point of the synchronization transition. (ii) The corresponding exponent values depend on the time bin Δt required to define avalanches, but (iii) fixing Δt to coincide with the inter-spike interval, ISI, the same statistics as in empirical networks, i.e. the critical exponents compatible with those of an unbiased branching process (10) are obtained. Finally (iv) scale-free distributions disappear if events are reshuffled in time, revealing a non-trivial temporal organization.

Thus, the main outcome of our analyses is that the underlying phase transition at which scale-free avalanches emerge does not separate a quiescent state from a fully active one; instead, it is a synchronization phase transition. This is a crucial observation, as most of the existing modeling approaches for critical avalanches in neural dynamics to date rely on a continuous quiescent/active phase transition.

Consistently with our findings– the amazingly detailed model put together by the Human Brain Project consortium suggests that the model best reproduces experimental features when tuned near to its synchronization critical point (89). In

such a study, the concentration of Calcium ions, Ca^{2+} needs to be carefully tuned to its actual nominal value to set the network state. Similarly, in our approach, the role of the calcium concentration is played by the parameter ξ, regulating the maximum level reachable by synaptic resources. Interestingly, the calcium concentration is well-known to modulate the level of available synaptic resources (i.e. neurotransmitter release from neurons; see e.g. (32, 58, 61)), hence, both quantities play a similar role.

Observe that here, we have not made any attempt to explore how could potentially the network self-organize to operate in the vicinity of the synchronization critical point without the need of parameter tuning. Adaptive, homeostatic and self-regulatory mechanisms accounting for this will be analyzed in future work. Also, here we have not looked for the recently uncovered *neutral neural avalanches* (40), as these require causality information to be considered, and such detailed causal relationships are blurred away in mesoscopic coarse grained descriptions.

Summing up, our Landau-Ginzburg theory with parameters lying in case (B) constitutes a sound description of the cortex during deep sleep or during anesthesia, when up and down transitions are observed. On the other hand, case (A) when tuned close to the synchronization phase transition can be a sound theory for the awaked cortex, in a state of alertness. A detailed analysis of how the transition between deep-sleep (described by case (B)) and awake (or REM sleep, described by case (A)) states may actually occur in these general terms is beyond our scope here, but observe that, just by modifying the speed at which synaptic resources recover it is possible to shift between the two cases, making it possible to investigate how such transitions could be induced.

A simple extension of our theory, including spatial heterogeneity has been shown to be able to reproduce remarkably well experimental measurements of activity in neural cultures with structural heterogeneity, opening the way to more stringent empirical validations of the general theory proposed here.

Even if further experimental, computational and analytical studies would be certainly required to definitely settle the controversy about the possible existence, origin, and functional meaning of the possible phases and phase transitions in cortical networks, we hope that the general framework introduced here –based on very general and robust principles– helps in clarifying the picture and in paving the way to future developments in this fascinating field.

Materials and Methods

Model details. In the Wilson-Cowan model, in its simplest form, the dynamics of the average firing rate or global activity, ρ, is governed by the equation

$$\dot{\rho}(t) = -a\rho\,(t) + (1-\rho(t))S\,(W\rho\,(t) - \Theta)$$

where W is the synaptic strength, Θ is a threshold value that can be fixed to unity, and $S(x)$ is a sigmoid (transduction) function, e.g. $S(x) = \tanh(x)$ (59, 60). We adopt this well-established model and, for simplicity, keep only the leading terms in a power-series expansion, and rename the constants, yielding the deterministic part of Eq.(1). To this we add noise $\sqrt{\rho(t)}\eta(t)$ –which is a delta-correlated Gaussian white noise of zero mean and unit variance, accounting for stochastic/demographic effects in finite local populations as dictated by the central limit theorem; a formal derivation of such an intrinsic or demographic noise, starting from a discrete microscopic model can be found in (59)). A noise term could be also added to the equation for synaptic resources (50), but it does not significantly affect the results. Considering N mesoscopic units, and coupling them diffusively within some networked structure (e.g. a two dimensional lattice), we finally obtained the set of Eqs.(3).

Analytic signal representation. The Hilbert transform $\mathcal{H}(\cdot)$ is a bounded linear operator largely used in signal analysis as it provides a tool to transform a given real-valued function $u(t)$ into a complex analytic function, called the *analytic signal representation*. This is defined as $\mathcal{A}_u(t) = u(t) + i\mathcal{H}[u(t)]$ where the Hilbert transform of $u(t)$ is given by: $\mathcal{H}[u(t)] = h * u = \frac{1}{\pi}\lim_{\epsilon\to 0}\int_{\epsilon}^{\infty}\frac{u(t+\tau)-u(t-\tau)}{\tau}d\tau$. Expressing the analytic signal in terms of its time-dependent amplitude and phase (polar coordinates) makes it possible to represent any signal as an oscillator. In particular, the associated phase is defined by $\phi_k^{\mathcal{A}} = \arctan Im(\mathcal{A}_k)/Re(\mathcal{A}_k)$.

From continuous timeseries to discrete events. Local timeseries at each single unit, $\rho_k(t)$, can be mapped into time sequences of point-like ("unit spiking") events. For this, a local threshold $\theta \ll 1$ is defined, allowing to assign a state on/off to each single unit/node (depending on whether it is above/below such a threshold) at any given time. If the threshold is low enough, the procedure is independent of its specific choice. A single (discrete) "event" or "spike" can be assigned to each node i, e.g. at the time of the maximal ρ_i within the on-state; a weight proportional to the integral of the activity time series spanned between two consecutive threshold crossings is assigned to each single event (see Fig.5A). Other conventions to define an event are possible, but results are not sensitive to it as illustrated in the SI6.

Phases from spiking patterns. An alternative method to define a phase at each unit can be constructed after a continuous timeseries has been mapped into a spiking series. In particular, using a linear interpolation: $\phi_k^{(\mathcal{B})}(t) = 2\pi(t-t_n^k)/(t_{n+1}^k - t_n^k)$ where $t \in [t_n^k, t_{n+1}^k)$ and t_n^k is the time of the n^{th} spike of node/unit k.

ACKNOWLEDGMENTS. We acknowledge the Spanish-MINECO grant FIS2013-43201-P (FEDER funds) for financial support. We are very thankful to P. Moretti, J. Hidalgo, J. Mejias, J.J. Torres, A. Vezzani, and P. Villa for useful suggestions and comments.

1. Arieli A, Sterkin A, Grinvald A, Aertsen A (1996) Dynamics of ongoing activity: explanation of the large variability in evoked cortical responses. *Science* 273(5283):1868.
2. Raichle ME (2011) The restless brain. *Brain. Connect.* 1(1):3–12.
3. Fox MD, Raichle ME (2007) Spontaneous fluctuations in brain activity observed with functional magnetic resonance imaging. *Nat. Rev. Neurosci.* 8(9):700–711.
4. Persi E, Horn D, Volman V, Segev R, Ben-Jacob E (2004) Modeling of synchronized bursting events: the importance of inhomogeneity. *Neural Comput.* 16(12):2577–2595.
5. Segev R, Shapira Y, Benveniste M, Ben-Jacob E (2001) Observations and modeling of synchronized bursting in two-dimensional neural networks. *Phys. Rev. E* 64(1):011920.
6. Buzsaki G (2009) *Rhythms of the Brain.* (Oxford Univ. Press, Oxford).
7. Beggs JM, Plenz D (2003) Neuronal avalanches in neocortical circuits. *J. of Neurosci.* 23(35):11167–11177.
8. Petermann T, et al. (2009) Spontaneous cortical activity in awake monkeys composed of neuronal avalanches. *Proc. Natl. Acad. Sci. USA* 106(37):15921–15926.
9. Binney J, Dowrick N, Fisher A, Newman M (1993) *The Theory of Critical Phenomena.* (Oxford Univ. Press, Oxford).
10. di Santo S, Villegas P, Burioni R, Muñoz M (2017) A simple unified view of branching process statistics: random walks in balanced logarithmic potentials. *Phys. Rev. E* 95(3):032115.
11. Mazzoni A, et al. (2007) On the dynamics of the spontaneous activity in neuronal networks. *PLoS One* 2(5):e439.
12. Pasquale V, Massobrio P, Bologna L, Chiappalone M, Martinoia S (2008) Self-organization and neuronal avalanches in networks of dissociated cortical neurons. *Neuroscience* 153(4):1354–1369.
13. Hahn G, et al. (2010) Neuronal avalanches in spontaneous activity in vivo. *J. Neurophysiol.* 104(6):3312–3322.
14. Haimovici A, Tagliazucchi E, Balenzuela P, Chialvo DR (2013) Brain organization into resting state networks emerges at criticality on a model of the human connectome. *Phys. Rev. Lett.* 110(17):178101.
15. Tagliazucchi E, Balenzuela P, Fraiman D, Chialvo DR (2012) Criticality in large-scale brain fMRI dynamics unveiled by a novel point process analysis. *Front. Physiol.* 3(15).
16. Shriki O, et al. (2013) Neuronal avalanches in the resting meg of the human brain. *J. Neurosci.* 33(16):7079–7090.
17. Bellay T, Klaus A, Seshadri S, Plenz D (2015) Irregular spiking of pyramidal neurons organizes as scale-invariant neuronal avalanches in the awake state. *Elife* 4:e07224.
18. Poil SS, Hardstone R, Mansvelder HD, Linkenkaer-Hansen K (2012) Critical-state dynamics of avalanches and oscillations jointly emerge from balanced excitation/inhibition in neuronal networks. *J. Neurosci.* 32(29):9817–9823.

19. Chialvo DR (2004) Critical brain networks. *Phys. A* 340(4):756–765.
20. Plenz D, Niebur E (2014) *Criticality in neural systems.* (John Wiley & Sons).
21. Chialvo DR (2010) Emergent complex neural dynamics. *Nat. Phys.* 6:744–750.
22. Mora T, Bialek W (2011) Are biological systems poised at criticality? *J. Stat. Phys.* 144(2):268–302.
23. Henkel M, Hinrichsen H, Lübeck S (2008) *Non-equilibrium Phase Transitions: Absorbing phase transitions*, Theoretical and mathematical physics. (Springer London, Berlin).
24. Marro J, Dickman R (2005) *Nonequilibrium Phase Transitions in Lattice Models*, Collection Aléa-Saclay. (Cambridge University Press).
25. Gireesh ED, Plenz D (2008) Neuronal avalanches organize as nested theta- and beta/gamma-oscillations during development of cortical layer 2/3. *Proc. Natl. Acad. Sci. USA* 105(21):7576–7581.
26. Yang H, Shew WL, Roy R, Plenz D (2012) Maximal variability of phase synchrony in cortical networks with neuronal avalanches. *J. Neurosci.* 32(3):1061–1072.
27. Levina A, Herrmann JM, Geisel T (2007) Dynamical synapses causing self-organized criticality in neural networks. *Nat. Phys.* 3(12):857–860.
28. de Arcangelis L, Perrone-Capano C, Herrmann HJ (2006) Self-organized criticality model for brain plasticity. *Phys. Rev. Lett.* 96(2):028107.
29. Millman D, Mihalas S, Kirkwood A, Niebur E (2010) Self-organized criticality occurs in non-conservative neuronal networks during/up/'states. *Nat. Phys.* 6(10):801–805.
30. Stepp N, Plenz D, Srinivasa N (2015) Synaptic plasticity enables adaptive self-tuning critical networks. *PLoS Comput. Biol.* 11(1).
31. Harnack D, Pelko M, Chaillet A, Chitour Y, van Rossum MC (2015) Stability of neuronal networks with homeostatic regulation. *PLoS Comput. Biol.* 11(7):e1004357.
32. Markram H, Tsodyks M (1996) Redistribution of synaptic efficacy between pyramidal neurons. *Nature* 382:807–810.
33. Shin CW, Kim S (2006) Self-organized criticality and scale-free properties in emergent functional neural networks. *Phys. Rev. E* 74(4):045101.
34. Dickman R, Muñoz M, Vespignani A, Zapperi S (2000) Paths to Self-Organized Criticality. *Braz. J. Phys.*
35. Bonachela JA, Muñoz MA (2009) Self-organization without conservation: true or just apparent scale-invariance? *J. Stat. Mech.* p. P09009.
36. Bak P (1996) *How nature works.* (Copernicus, New York).
37. Jensen HJ (1998) *Self-organized criticality: emergent complex behavior in physical and biological systems.* (Cambridge university press, Cambridge).
38. de Arcangelis L (2012) Are dragon-king neuronal avalanches dungeons for self-organized brain activity? *Eur. Phys. J. Spec.Top.* 205(1):243–257.
39. Bonachela J, de Franciscis S, Torres J, Muñoz MA (2010) Self-organization without conservation: are neuronal avalanches generically critical? *J. Stat. Mech.Theory E.* 2010(02):P02015.
40. Martinello M, et al. (2017) Neutral theory and scale-free neural dynamics. *Physical Review X.*
41. Van Vreeswijk C (1996) Partially synchronized states in networks of pulse-coupled neurons. *Phys. Rev. E* 54:5522–5537.
42. Amit DJ, Brunel N (1997) Model of global spontaneous activity and local structured activity during delay periods in the cerebral cortex. *Cereb. Cortex* 7(3):237–252.
43. Brunel N (2000) Dynamics of sparsely connected networks of excitatory and inhibitory spiking neurons. *J. Comput. Neurosci.* 8(3):183–208.
44. Brunel N, Hakim V (2008) Sparsely synchronized neuronal oscillations. *Chaos* 18(1):015113.
45. Gautam SH, Hoang TT, McClanahan K, Grady SK, Shew WL (2015) Maximizing sensory dynamic range by tuning the cortical state to criticality. *PloS Comput. Biol.* 11(12):e1004576.
46. Touboul J, Destexhe A (2017) Power-law statistics and universal scaling in the absence of criticality. *Phys. Rev. E* 95(1):012413.
47. Destexhe A (2009) Self-sustained asynchronous irregular states and up down states in thalamic, cortical and thalamocortical networks of nonlinear integrate-and-fire neurons. *J. Comput. Neurosci.* 27(3):493–506.
48. Steriade M, Nunez A, Amzica F (1993) A novel slow (< 1 hz) oscillation of neocortical neurons in vivo: depolarizing and hyperpolarizing components. *J. Neurosci.* 13(8):3252–3265.
49. Holcman D, Tsodyks M (2006) The emergence of up and down states in cortical networks. *PLoS Comput. Biol.* 2(3):e23.
50. Mejias JF, Kappen HJ, Torres JJ (2010) Irregular dynamics in up and down cortical states. *PLoS One* 5(11):e13651.
51. Stanley HE (1987) *Introduction to phase transitions and critical phenomena.* (Oxford University Press, Oxford).
52. Toner J, Tu Y, Ramaswamy S (2005) Hydrodynamics and phases of flocks. *Ann. Phys.* 318(1):170–244.
53. Villa Martín P, Bonachela JA, Levin SA, Muñoz MA (2015) Eluding catastrophic shifts. *Proc. Natl. Acad. Sci. USA* 112(15):E1828–E1836.
54. Buice MA, Cowan JD (2007) Field-theoretic approach to fluctuation effects in neural networks. *Phys. Rev. E* 75(5):051919.
55. Bressloff PC (2010) Metastable states and quasicycles in a stochastic wilson-cowan model of neuronal population dynamics. *Phys. Rev. E* 82(5):051903.
56. Bressloff PC (2012) Spatiotemporal dynamics of continuum neural fields. *J. Phys. A Math. Theor.* 45(3):033001.
57. Kandel ER, Schwartz JH, Jessell TM, Siegelbaum SA, Hudspeth AJ (2000) *Principles of neural science.* (McGraw-hill New York) Vol. 4.
58. Dayan P, Abbott L (2003) Theoretical neuroscience: computational and mathematical modeling of neural systems. *J. Cogn. Neurosci.* 15(1):154–155.
59. Benayoun M, Cowan JD, van Drongelen W, Wallace E (2010) Avalanches in a stochastic model of spiking neurons. *PLoS Comput. Biol.* 6(7):e1000846.
60. Wilson HR, Cowan JD (1972) Excitatory and inhibitory interactions in localized populations of model neurons. *Biophys. J.* 12(1):1–24.
61. Tsodyks M, Markram H (1997) The neural code between neocortical pyramidal neurons depends on neurotransmitter release probability. *Proc. Natl. Acad. Sci. USA* 94:719–723.
62. Mattia M, Sanchez-Vives MV (2012) Exploring the spectrum of dynamical regimes and timescales in spontaneous cortical activity. *Cogn. Neurodyn.* 6(3):239–250.
63. Levina A, Herrmann JM, Geisel T (2009) Phase transitions towards criticality in a neural system with adaptive interactions. *Phys. Rev. Lett.* 102(11):118110.
64. Deco G, Jirsa VK (2012) Ongoing cortical activity at rest: criticality, multistability, and ghost attractors. *J. Neurosci.* 32(10):3366–3375.
65. Gardiner C (2009) *Stochastic Methods: A Handbook for the Natural and Social Sciences*, Springer Series in Synergetics. (Springer).
66. Breakspear M (2017) Dynamic models of large-scale brain activity. *Nature neuroscience* 20(3):340–352.
67. Deco G, Jirsa VK, Robinson PA, Breakspear M, Friston K (2008) The dynamic brain: from spiking neurons to neural masses and cortical fields. *PLoS Comput. Biol.* 4(8):e1000092.
68. Sporns O (2010) *Networks of the Brain.* (MIT Press, USA).
69. Torres JJ, Varona P (2012) Modeling biological neural networks in *Handbook of Natural Computing.* (Springer), pp. 533–564.
70. Yu S, Klaus A, Yang H, Plenz D (2014) Scale-invariant neuronal avalanche dynamics and the cut-off in size distributions. *PloS one* 9(6):e99761.
71. Dornic I, Chaté H, Muñoz MA (2005) Integration of langevin equations with multiplicative noise and the viability of field theories for absorbing phase transitions. *Phys. Rev. Lett.* 94(10):100601.
72. Hobbs JP, Smith JL, Beggs JM (2010) Aberrant neuronal avalanches in cortical tissue removed from juvenile epilepsy patients. *J. Clin. Neurophysiol.* 27(6):380–386.
73. da Silva FL (1991) Neural mechanisms underlying brain waves: from neural membranes to networks. *Electroencephalogr. Clin. Neurophysiol.* 79(2):81–93.
74. Tabak J, Senn W, O'Donovan MJ, Rinzel J (2000) Modeling of spontaneous activity in developing spinal cord using activity-dependent depression in an excitatory network. *Journal of Neuroscience* 20(8):3041–3056.
75. Peng C, Havlin S, Stanley HE, Goldberger AL (1995) Quantification of scaling exponents and crossover phenomena in nonstationary heartbeat time series. *Chaos: An Interdisciplinary Journal of Nonlinear Science* 5(1):82–87.
76. Linkenkaer-Hansen K, Nikouline VV, Palva JM, Ilmoniemi RJ (2001) Long-range temporal correlations and scaling behavior in human brain oscillations. *Journal of Neuroscience* 21(4):1370–1377.
77. Pikovsky A, Rosenblum M, Kurths J (2003) *Synchronization: a universal concept in nonlinear sciences.* (Cambridge university press, Cambridge) Vol. 12.
78. Jbabdi S, Sotiropoulos SN, Haber SN, Van Essen DC, Behrens TE (2015) Measuring macroscopic brain connections in vivo. *Nat Neurosci* 18(11):1546–1555.
79. Okujeni S, Kandler S, Egert U (2017) Mesoscale architecture shapes initiation and richness of spontaneous network activity. *Journal of Neuroscience* 37(14):3972–3987.
80. Moretti P, Muñoz MA (2013) Griffiths phases and the stretching of criticality in brain networks. *Nat. Comm.* 4.
81. Freeman WJ (1975) *Mass action in the nervous system.* (Elsevier Science & Technology, New York).
82. David O, Friston KJ (2003) A neural mass model for meg/eeg:: coupling and neuronal dynamics. *NeuroImage* 20(3):1743–1755.
83. El Boustani S, Destexhe A (2009) A master equation formalism for macroscopic modeling of asynchronous irregular activity states. *Neural Comput.* 21(1):46–100.
84. Gerstner W, Kistler WM, Naud R, Paninski L (2014) *Neuronal dynamics: From single neurons to networks and models of cognition.* (Cambridge University Press, Cambridge).
85. Täuber UC (2014) *Critical dynamics: a field theory approach to equilibrium and non-equilibrium scaling behavior.* (Cambridge University Press).
86. Pittorino F, Ibáñez Berganza M, di Volo M, Vezzani A, Burioni R (2017) Chaos and correlated avalanches in excitatory neural networks with synaptic plasticity. *Phys. Rev. Lett.* 118(9):098102.
87. Cabral J, Hugues E, Sporns O, Deco G (2011) Role of local network oscillations in resting-state functional connectivity. *Neuroimage* 57(1):130–139.
88. Villegas P, Moretti P, Muñoz MA (2014) Frustrated hierarchical synchronization and emergent complexity in the human connectome network. *Sci. Rep.* 4:5990.
89. Markram H, et al. (2015) Reconstruction and simulation of neocortical microcircuitry. *Cell* 163(2):456–492.

Supporting Information: Landau-Ginzburg theory of cortical dynamics: scale-free avalanches emerge at the edge of synchronization

Serena di Santo[a,b,c,1], **Pablo Villegas**[a,1], **Raffaella Burioni**[b,c], **and Miguel A. Muñoz**[a,2]

[a]Departamento de Electromagnetismo y Física de la Materia e Instituto Carlos I de Física Teórica y Computacional. Universidad de Granada. E-18071, Granada, Spain; [b]Dipartimento di Fisica e Scienza della Terra, Università di Parma, via G.P. Usberti, 7/A - 43124, Parma, Italy; [c]INFN, Gruppo Collegato di Parma, via G.P. Usberti, 7/A - 43124, Parma, Italy

SI1. Robustness of the results against changes in the dynamics. In this appendix we confirm the robustness of the results and conclusions presented in the main part with respect to the modification of diverse ingredients and modeling details. In particular, we *first* discuss the full model including synaptic plasticity (as in the main text), but without truncating the equation for activity in a series expansion and, *second*, we consider inhibition as encapsulated in the well-known Wilson-Cowan equations (rather than synaptic plasticity) as a chief regulatory mechanism.

Non-truncated excitatory-activity equation. The dynamics in a single mesoscopic region of the cortex or "unit" is described by the full Wilson-Cowan equation (1) for the excitatory activity –such that the activity grows with the incoming current through a sigmoid response function– together with the Tsodyks-Markram TM model for synaptic plasticity (2):

$$\begin{cases} \dot{\rho} = & -a\rho + (1-\rho)\tanh\left(\rho R - \Theta\right) + h \\ \dot{R} = & \frac{1}{\tau_R}\left(\xi - R\right) - \frac{1}{\tau_D}\rho R. \end{cases} \quad [1]$$

In Figure 1, we illustrate that a linear-stability analysis reproduces a Hopf bifurcation scenario, as in the most relevant case (case A) discussed in the paper. When noise and spatial coupling are added, and the system is studied on a two-dimensional lattice, a synchronous irregular regime of network spikes, as well as an asynchronous irregular regime of nested oscillations –fully analogous to their corresponding counterparts in the the main text– are found, as graphically illustrated by the lower panels of Figure 1. This unveils the existence of a synchronization transition and confirms that the simplified truncated equation for the activity considered in the main text is a valid approximation of the full dynamics. Here we do not show a detailed analysis of the synchronization transition nor of the emergence of scale-free avalanches; but, let us remark that we have not found any substancial qualitative difference with respect to the case discussed in the paper in any of our exploratory checks.

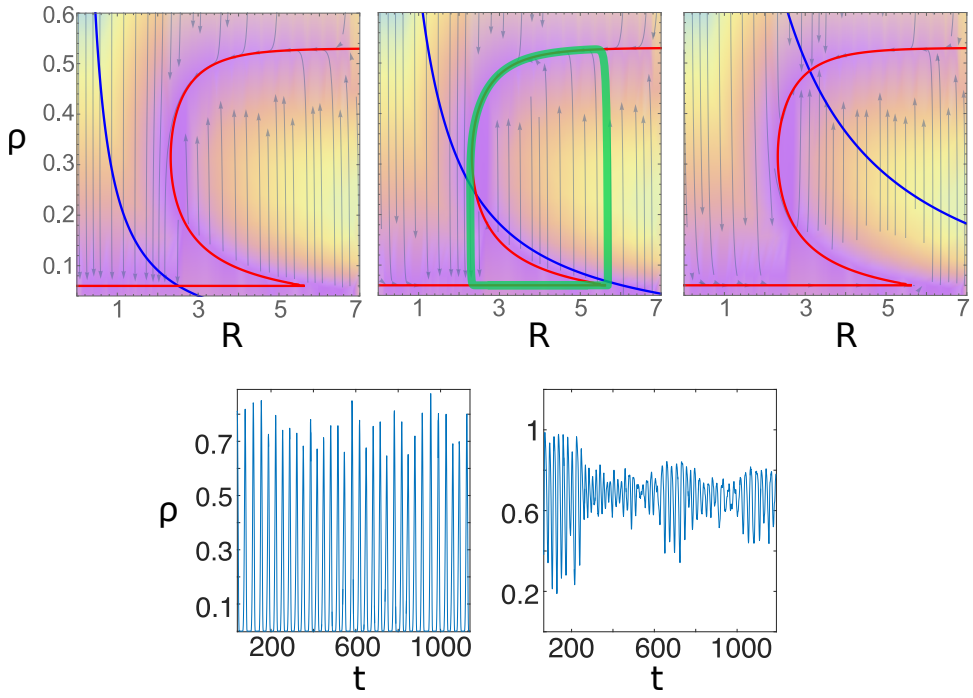


Fig. 1. Analysis of the model of Eq. 1. Upper panels: deterministic phase portrait with $\xi = 5, 12, 28$ (from left to right). respectively. showing a down state, a limit cycle and up state regimes, as in the case A of the main text. Other parameters are $a = 1$, $\tau_D^{-1} = 0.033$, $\tau_R = 500$, $\Theta = 0.34$, $h = 0.06$. Varying parameter values, it is possible to find either a similar Hopf bifurcation (case A) or a saddle node bifurcation (case B), as in the model with the truncated expansion. Lower panels: Temporal evolution of the total activity $\rho(t)$ on a two-dimensional lattice with $N = 64^2$ (after having introduced noise and coupling); in the (left) synchronous (network spiking) and in the (right) asynchronous (nested oscillations) regimes, respectively, revealing the presence of a synchronization phase transition in between the two regimes; parameter values: $\xi = 5$ and $\xi = 13$, respectively.

Inhibition as main regulatory mechanism. In this section we consider the full Wilson-Cowan equations (1), including both excitatory and inhibitory neural populations for each mesoscopic region or unit. In this case, inhibition plays the role of chief homeostatic mechanism, regulating the level of the overall network activity. More specifically, we consider a version of the Wilson-Cowan

dynamics, including also intrinsic noise as corresponds to large but finite (mesoscopic) regions. Such a model has been recently derived from an underlying microscopic model of spiking neurons in Ref. (3), and is described by the following set of stochastic equations for the densities of excitatory (E) and inhibitory (I) neurons:

$$\begin{aligned}\dot{E}_i &= -\alpha E_i + (1-E_i)\tanh\left[\omega_{EE}E_i - \omega_{IE}I_i + h\right] + \sigma\sqrt{\alpha E_i + (1-E_i)\tanh\left[\omega_{EE}E_i - \omega_{IE}I_i + h\right]} \\ \dot{I}_i &= -\alpha I_i + (1-I_i)\tanh\left[\omega_{EI}E_i - \omega_{II}I_i + h\right] + \sigma\sqrt{\alpha I_i + (1-I_i)\tanh\left[\omega_{EI}E_i - \omega_{II}I_i + h\right]}\,, \end{aligned} \quad [2]$$

where α is the decay rate for the activity, h is an external driving field, σ is the noise amplitude, and ω_{ij} (with $i,j = E,I$) are the couplings between population i and j within a single unit; particularly important here is the auto-excitation coupling ω_{EE}, which we take as a control parameter.

First of all, these equations are analyzed in the (noiseless) mean field limit. By increasing ω_{EE}, the system exhibits a transition from a "down" state to an "up" state (see Fig. 2). Thus, a saddle-node bifurcation separates a state of high activity from a state of low activity, we found no track of a possible Hopf bifurcation. However, as soon as noise is switched on (i.e $\sigma \neq 0$), a noise-induced phenomenon appears: trajectories nearby the up-state fixed point, can escape from its basin of attraction as a result of fluctuations, and are then almost deterministically driven towards the down state, where a similar mechanism makes them escape with some probability. This phenomenon has been recently scrutinized in a remarkable work, where the role of non-normal forms in generating complex dynamics in general and avalanches in particular, has been emphasized (3).

This mechanism, generates in an effective way a noise-induced limit cycle between up and down states, which plays the same role as the deterministic limit cycle (Hopf bifurcation) of case A described in the main text. As a matter of fact, computer simulations of units described by Eq.(2), and coupled diffusively, give rise to the phenomenology illustrated in Fig.2: as the control parameter ω_{EE} is increased, the system undergoes a phase transition from a synchronous phase with very distinctive network spikes, to an asynchronous regime with nested oscillations, as it happens in the model with synaptic plasticity. Thus, also in this case, the phases are the same as in the main text and a synchronization transition appears between them.

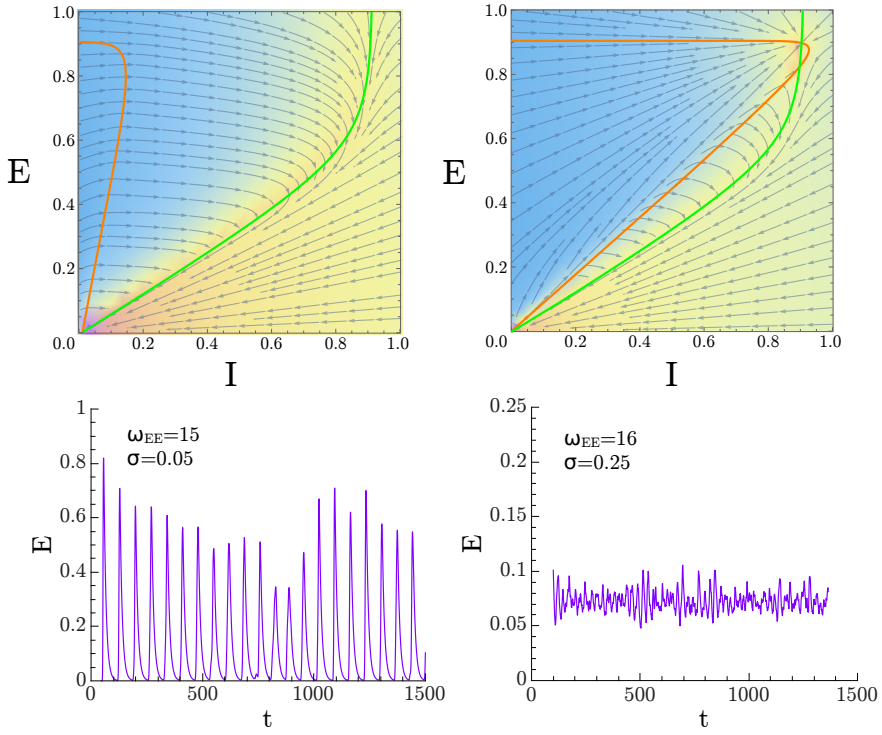


Fig. 2. Upper panels: mean-field analysis of the Wilson-Cowan set of Eqs. (2) describing both excitatory and inhibitory neural populations at each single unit, with parameters such that a noise-induced limit cycle (see (3)) in between a down and an up state can emerge once a non-vanishing noise is switched on. Observe that there is (left) a stable down-state fixed point ($\omega_{EE} = 4$) and a (right) stable up state ($\omega_{EE} = 16$); however the basin of attraction of the up state is small, and a relatively small fluctuation can induce the system state to go beyond the saddle-node line, where deterministic trajectories take the system toward the down state. In the lower panels we illustrate results of a computer simulation for a two-dimensional lattice of coupled noisy units, Eq.(2), corresponding to (left) synchronous/network-spiking and (right) asynchronous/nested-oscillation regimes. Parameter values: $D = 1, \omega_{EI} = 4.65, \omega_{IE} = 14.0, \omega_{II} = 2.8, h = 10^{-3}$ and $\alpha = 0.1$. Control parameter $\omega_{EE} = 15$ for SI regime and $\omega_{EE} = 16$.

SI2. Robustness against changes in synaptic time scales, diffusion and noise. As discussed in the main text, there are two possible scenarios according to the relation between the timescales for the recovery and depletion (τ_R and τ_D, respectively). Namely, between the quiescent or 'down' state with $\rho^* \approx 0$ and the active or 'up' state with self sustained activity there exists a stable limit cycle (case A) or a regime of bistability (case B). Fixing parameter values while changing τ_R and τ_D, it is possible to construct (mean-field or deterministic) a phase diagram showing the different possible cases that emerge when the control parameter ξ is varied (cases A and B). As shown in Fig. 3 when the recovery time (τ_R) is much bigger than the depletion time (τ_D) the system is in the case A, while for bigger values of the depletion time (τ_D) it falls into the case B with a transitions between up (active) and down (quiescent) states.

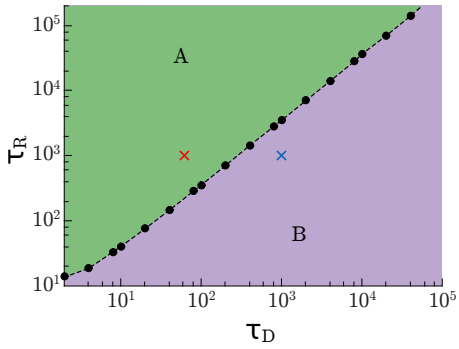


Fig. 3. Mean-field phase diagram showing the type of transition for different values of τ_R and τ_D. Red (blue) cross show the particular case chosen in the Fig.1 of the main text for the case A (B). Parameter values are $a = 0.6, b = 1.3, h = 10^{-3}$.

We have also explored the behavior of the system against changes in the diffusion constant D. Figure 4 shows the phase diagram for different values of D and some particular temporal series with the aim of characterize the different possible behaviors. As can be observed, there exists a transition from the synchronous irregular phase to the synchronous regular one for a wide range of D values (.e.g. from $D = 0.01$ (red line) to $D = 2$ (violet line), and $D = 4$ (green line)). If D is set to very large values, the system falls into the mean field expected behavior, switching from the network spiking regime to the up state. Similar conclusions are obtained, by fixing D and decreasing the noise amplitude σ.

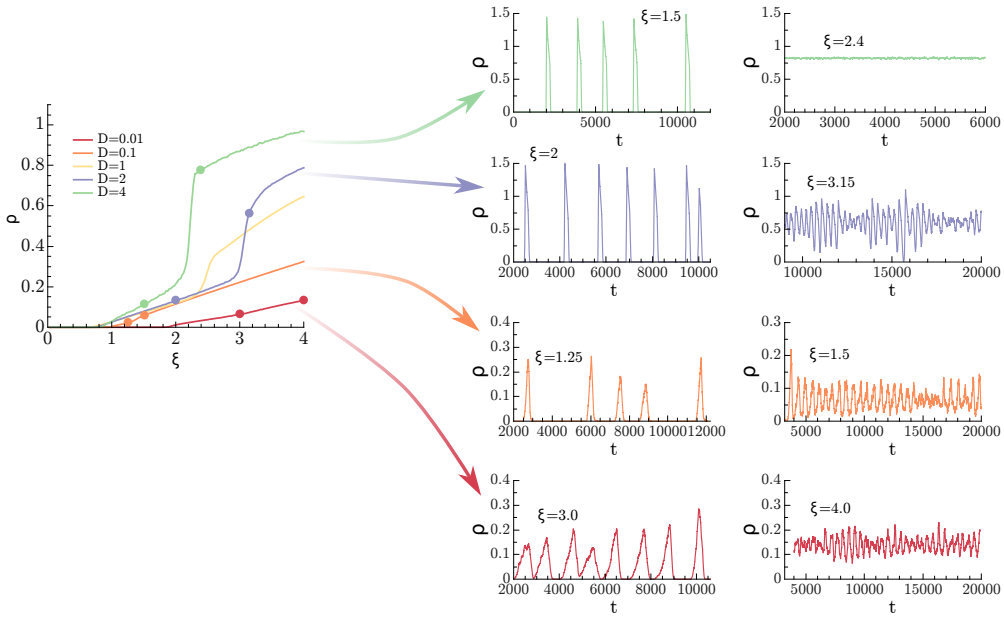


Fig. 4. Left panel: Order parameter as a function of the control parameter ξ for various values of the diffusion constant D. Right panel: Temporal series for two particular values of ξ for each value of D, (marked with colored points in the left panel), showing the expected behavior. Low values of D show a transition between the synchronous irregular phase to the asynchronous irregular one, as in the main text (red, orange, violet and green line). Parameter values: $a = 1.0, b = 1.5, \tau_R = 10^3, \tau_D = 10^2, h = 10^{-7}$.

SI3. The effect of long-range connections and network heterogeneity. The detailed map of synaptic connections plays a central role in brain function (4). Even if most of the neuronal connections occur within the local neighborhood, long-range white-matter connectivity allows for information to be distributed and processed across the whole cortex. Such long-range connections comprise only about 10% of the total connections in the brain, but their role is crucial for brain functionality (4, 5).

Small-world topology. As the simplest possible approximation beyond a lattice of nearest neighbor connections, and consistently with (5), we built a small-world network, as done in the Watts-Strogatz model (6), by rewiring 10% of the links of a two-dimensional lattice. We explored the phase space of the model defined by Eqs. 1 and 2 of the main text, on this connectivity architecture (see Fig.(5) upper panel), and observed that the leading features described in the paper (i.e. phases and phase transitions) are preserved when long-range interactions are introduced. Indeed, as illustrated in the lower part of Fig.(5), our computational analyses reveal that the emergence of synchronous and an asynchronous phase, with a synchronization transition in between is a general intrinsic feature of our model, which is not modified by the small-world property of the network.

In any case, it is important to remark that even if the main phases remain unaffected, important details such as the extension of such phases, the specific shape of avalanches, the amplitude of nested oscillations, the broadness of the critical-like region etc. could be potentially sensitive to the introduction of network heterogeneity. Some of these aspects are explicitly illustrated in the forthcoming paragraphs.

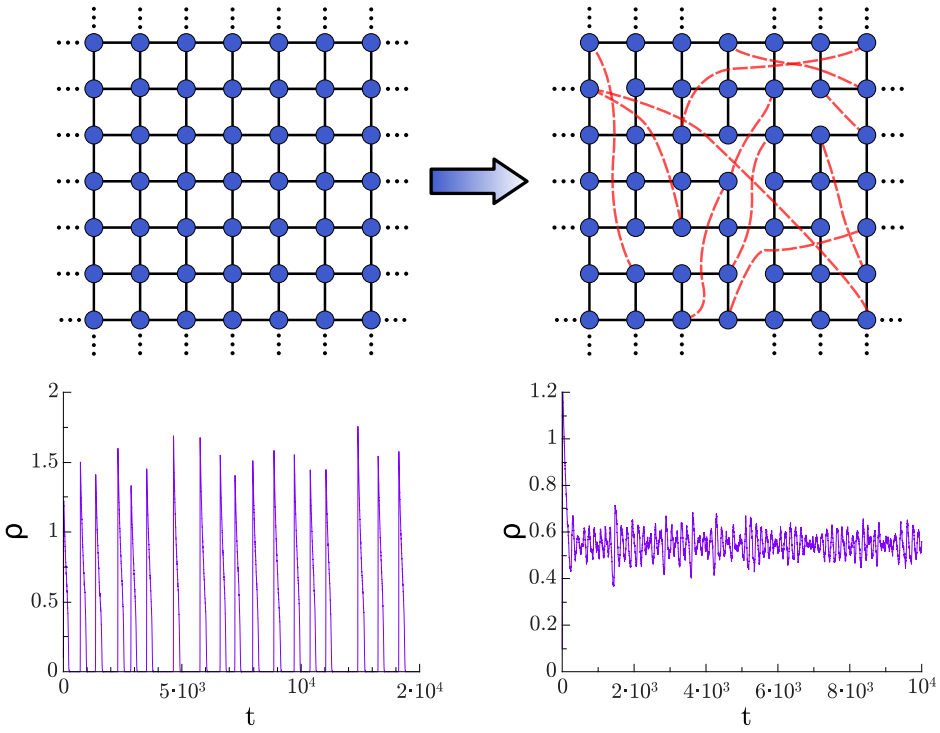


Fig. 5. Upper panel: sketch of the rewiring procedure defining a small-world network architecture: a ten percent of the links are rewired, in such a way that the average connectivity is preserved. Lower panel: Plots illustrating the results of computational analyses of the dynamics (main text, Eq. 1 and 2); in particular, temporal series of the global electrical activity in a small world lattice for two different values of control parameter ξ; (left, $\xi = 2.8$) synchronous/network-spike regime, and (right, $\xi = 2.96$) asynchronous/nested-oscillation regimes, respectively; a synchronization phase transition exists separating these two alternative regimes. Other parameter values: $a = 1.0, b = 1.5, \tau_D = 10^2, \tau_R = 10^3, h = 10^{-7}$.

Clustered and heterogeneous networks. Recent experimental analyses have scrutinized the effect of network heterogeneity in cultures of rat cortical neurons *in vitro* (7). In particular, Okujeni *et al.* where able to control the level of clustering by experimentally modifying the level of a given enzyme (protein Kinase C) that promotes neuronal aggregation. In this way, progressively more clustered networks were generated as the level of protein was increased (see Fig. 1 in (7)).

Keeping fixed other experimental conditions, Okujeni *et al.* found that in the case in which neurons are more homogeneously distributed in the substrate networks spikes appear much more sporadically than when the network is highly clustered (see Fig. 7, which is adapted from (7)), and that network spikes appear more clustered in time in this latter case. Thus, in conclusion, clustering promotes the generation of spontaneous network activity.

In order to model these experimental results, we developed a heterogeneous network in which we keep fixed the mean value of the parameter a (that controls the decay of the activity at each single unit), but inducing some areas with low local values of a_1, i.e. with a smaller propensity for activity to decay (red nodes in Fig. 6), while in the rest of the network larger values of a, a_2, are considered (keeping the network-average value of a constant).

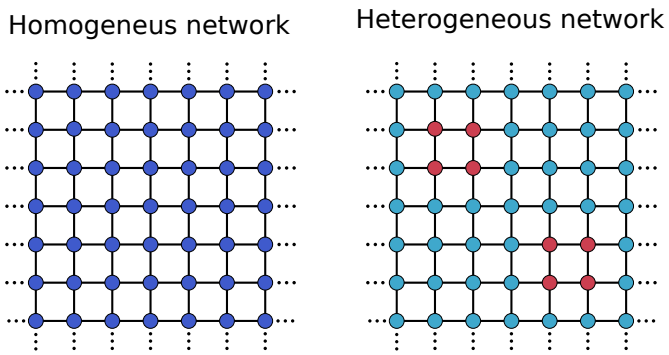


Fig. 6. Sketch of the considered networks: homogeneous to the left and heterogeneous/clustered to the right. In both cases the network-average value of the activity-decay parameter a is taken to be equal. However, while in the homogeneous case the value of a is constant across the network, in the heterogeneous one there are some areas (marked with red nodes) with a lower value of a.

As shown in Figure 7, the lower the local value of a_1, the more facilitated the emergence of spontaneous activity, leading the system closer and closer to the critical point or the asynchronous irregular phase, and reproducing quite remarkably the chief experimental observations of Okujeni *et al.*

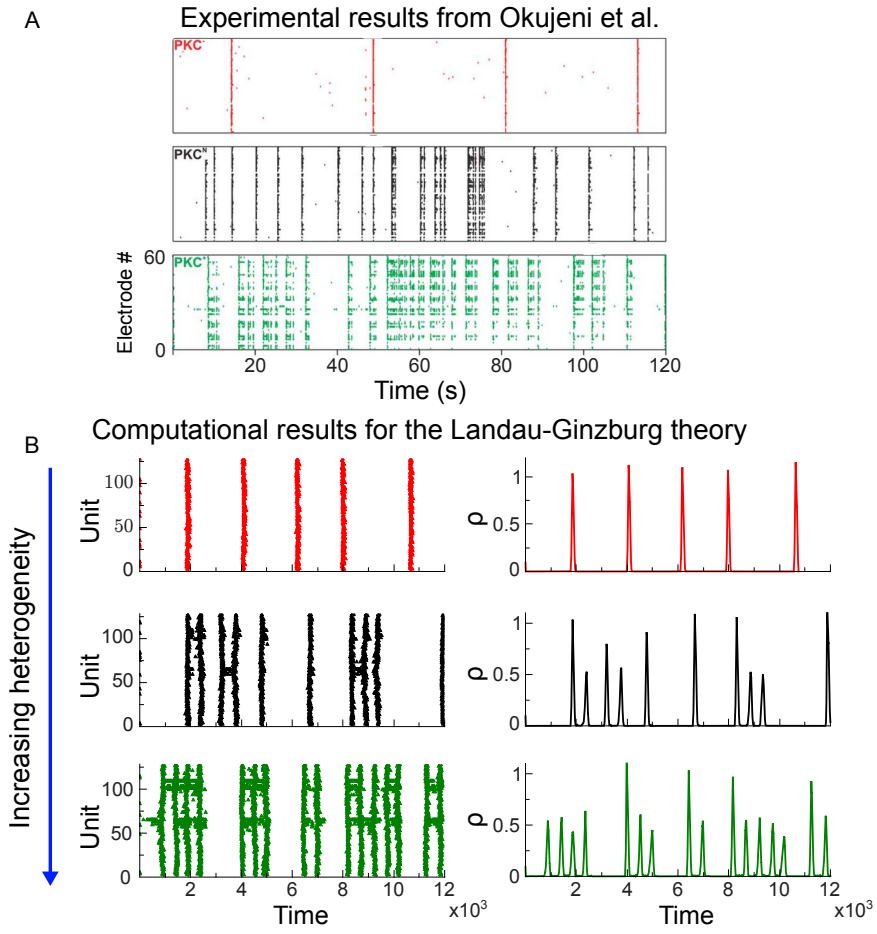


Fig. 7. Temporal series for different level of network clustering. Panel A shows the experimental results of Okujeni (7) (adapted figure from the original paper) for increasing levels of aggregation in a neural network. Panel B shows three temporal series for different levels of network clustering and a fixed value of $\xi = 1.2$. In the first one (red) the network is homogeneous with $a_1 = a_2 = 1$. Observe that smaller values of a_1 produce a more active network, in particular for $a_1 = -0.7$ (black) and $a_1 = -0.928$ (green). In both cases, the clustering facilitate the spontaneous activity. Other parameter values: $b = 1.5, \tau_D = 10^2, \tau_R = 10^3, h = 10^{-7}$.

Thus, in conclusion, our general model, equipped with an additional layer of network heterogeneity is able to reproduce specific empirical results.

SI4. Detrended Fluctuation Analysis. In this section we present an additional type of analyses to discriminate whether the system lays at a critical point or in either the subcritical or the supercritical phases. The method is based on the fact that, at the critical point of a continuous phase transition, the (time-dependent) order parameter, as measured in any finite system, shows long-range temporal correlations (i.e. long-memory effects), which can be quantified by measuring its Hurst exponent (8). The Hurst exponent of a time series is a measure of the dispersion of a process on a scaling support. For example the Hurst exponent of an uncorrelated signal (white noise) is $\alpha = 1/2$, since the root mean square translation distance after n steps of a Wiener process, i.e. an unbiased random walk (the process obtained by integrating white noise), is proportional to $\sqrt{n}$. For correlated signals (colored noises) one expects bigger Hurst exponents (as a reference, $\alpha \simeq 1$ is found for pink noise). The Hurst exponent can be calculated by splitting the time series into adjacent windows, plotting the square-root displacement from the mean as a function of the window size and evaluating the exponent of the resulting power law (see below). More specifically, "detrended fluctuation analysis" (DFA) is a technique for measuring the Hurst exponent in non-stationary time series: the "detrending" operation allows to remove fictitious memory effects related to non-stationarity, and the method basically consists in subtracting the local "trend" (usually using a linear fit approximation) of the signal before performing the analysis on each window (9, 10). DFA consists of two steps: the data series $\rho(t)$ is shifted by its mean $\bar{\rho}$, and integrated (cumulatively summed) in time:

$$\mathcal{P}(\tau) = \sum_{t=1}^{\tau} \left(\rho(t) - \bar{\rho}\right); \qquad [3]$$

then segmented into k windows of various sizes n, and for each window size, a fluctuation function $F(n)$ is calculated, as

$$F(n) = \sqrt{\frac{1}{T}\sum_{h=1}^{k}\sum_{\tau=1}^{n}\left(\mathcal{P}^{(n)}(\tau + (h-1)n) - X_{\mathcal{P}}^{(n)}\right)^2} \qquad [4]$$

where $X_{\mathcal{P}}^{(n,h)}$ is the linear regression of $\mathcal{P}^{(n)}(\tau)$, with $\tau \in [(h-1)n, hn]$, the superscript indicates the dependence on the window size n and $T = kn$ is the total length of the time series. If $F(n) \sim n^{-\alpha}$, then α is the Hurst exponent (9, 11).

We performed a DFA on the global signal $\rho(t)$ coming out of our computer simulations for different values of the control parameter ξ (in the synchronous and asynchronous phases as well as at the critical point). Results are shown in Fig.8: (i) fluctuations in the asynchronous phase grow approximately as the square root of the window length, as expected for (uncorrelated) white noise; (ii) in the synchronous phase, above a certain characteristic length, the dependence is very weak, remarking the existence of a certain degree of order, i.e. a characteristic time scale at which there is order, i.e. synchronization; (iii) just at the critical point the growth of the fluctuations is anomalously large, confirming the existence of long-range correlations: a signature of criticality. Therefore, from the global activity signal we are able –through a DFA analysis– to conclude that long-range correlations, characteristic of criticality, emerge at the transition point.

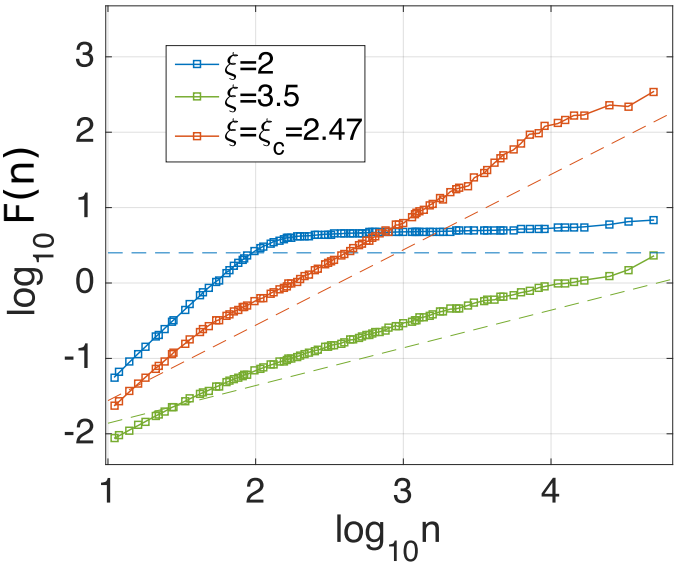


Fig. 8. Detrended fluctuation analysis of the macroscopic signal for different values of the control parameter $\xi = 2$ (synchronous phase) $\xi = 2.47$ (critical point), and 3.5 (asynchronous phase), respectively. Close to the transition point the DFA shows an Hurst exponent close to 1 (orange dashed line) implying long-range autocorrelations, a fingerprint of criticality, while the white noise value $\alpha = 1/2$ (green dashed line) emerges in the asynchronous regime, and an asymptotically almost flat curve is obtained in the synchronous phase, revealing the existence of a characteristic time scale. Parameter values are taken as in the main text and $N = 2^{14}$.

SI5. The nature of nested oscillations. In order to unveil the nature of the nested oscillation (asynchronous irregular, (AI)) phase and to determine whether it is a finite size effect or it survives in the thermodynamic limit, the existence of a second phase transition separating it from the up state is investigated here. In other words: are the asynchronous irregular phase and the up-state phase two different phases, or are they just the same phase, with only a quantitative difference in the amplitude of the variability around the mean value? As we illustrate in what follows the correct answer is this second one.

In principle, these two regimes show a qualitative difference: in the AI phase each single unit keeps switching between the *on/up* and *off* states and there exists a macroscopic fraction of *off/down* sites, whereas in the active phase units are permanently in the *on* state and, even if fluctuations might lead some unit to the *off* state, the macroscopic fraction of them vanishes (see Supplementary Movie). The fraction of inactive units, ρ_0, can thus be chosen as an order parameter for the putative phase transition between the AI and the active phase. In Figure 9 we plot the average over time of ρ_0 in function of ξ and we verify that this alternative order parameter detects the same phase transition already characterized in the main text, by employing synchronization order parameters. This implies that, in the large system-size limit, there exists no macroscopic difference between the asynchronous/nested-oscillation regime and the up state. Therefore, the nested oscillations can be understood as the result of partial synchronization of local regions; the superposition of a few regions gives rise to complex waves as those in Fig.2 (A3) of the main text. However, when the system becomes progressively large, the number of such locally synchronized regions grows, and their interference leads to a standard up state, in which fluctuations around the mean density decay as a function of the system size.

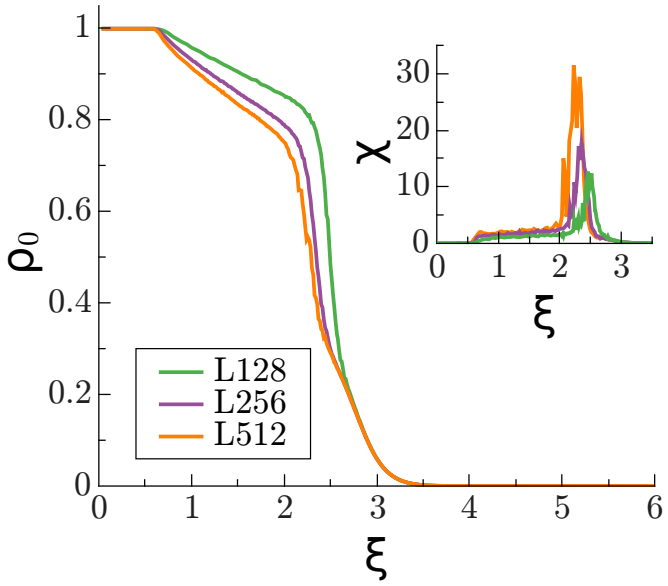


Fig. 9. Main: averaged fraction of inactive sites in the system ρ_0 as a function of the control parameter ξ, revealing the presence of a phase transition. Inset: Variance over runs of a given fixed duration of the average value of the control parameter multiplied by $\sqrt{N}$ in order to highlight possible deviations with respect to central limit theorem (CLT); as a result of which, a decay with $\sqrt{N}$ is expected; thus multiplying by $\sqrt{N}$ a convergence to a constant should be expected if the CLT holds. Observe, however, the increase in peak height as the system size is enlarged revealing a violation of the CLT, as expected at the critical point of a second order phase transition. Note that for all the system sizes the peaks are located approximately in the same spots as in Fig.4 in the main text; thus ρ_0 is an alternative order parameter that leads to the same results as the previously considered synchronization order parameters: it detects the synchronization phase transition, and reveals that there is no difference between the AI and the active phase in the limit of infinitely-large network sizes.

SI6. Definition and analyses of avalanches.

On the definition of spiking events. In the analysis of avalanches presented in the main text, a particular (and reasonable) criterion has been chosen to convert each local (continuous) time signal into a discrete series of spikes, allowing to build up the raster plot, from which avalanches are measured using the standard experimental protocol consisting on a time-clustering the events (12).

Here, we employ a different criterion to define spikes, thereby illustrating the robustness of our main findings against such a choice. In particular, the alternative discretization criterion is sketched in Figure 10 and is as follows: a threshold θ is established at each single unit, and every unit is declared to be in its *spiking* (or "on") state whenever its activity is over threshold. Thus, the main difference with the protocol in the main text is that now, in between two-consecutive time steps in which the unit is below threshold, the site is considered to be "on" not just at one time step (at its maximum of activity, as in the method of the main text), but possibly during many time steps, in a full time interval.

Considering these spiking events, avalanches are defined through the same experimentally inspired protocol that we used in the main text; the size of an avalanche is simply the number of spike counts during an avalanche. Figure 10 shows that the avalanche size distribution at the critical point is preserved by employing this alternative definition of the spikes. Moreover if a (random) subsampling of the units is performed, the distribution keeps following a power law which is roughly consistent with the experimentally measured exponent $3/2$.

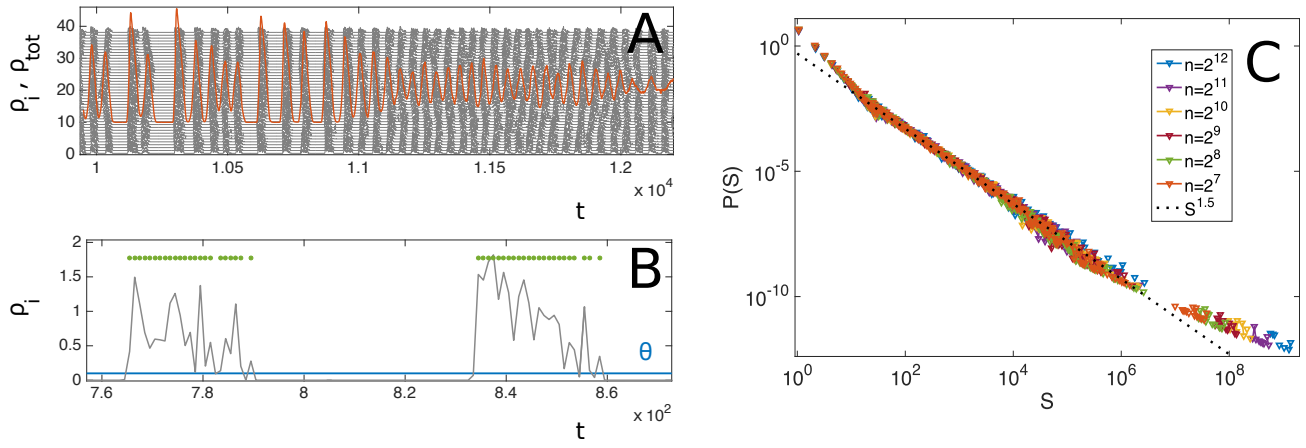


Fig. 10. A. Sample of local temporal signals are plotted in grey (shifted for convenience of visualization) together with the global signal $\rho(t)$ (shifted and rescaled) represented in red color, for a lattice of $N = 64^2$ units. B. illustration of the alternative method employed here to define "spike events" from a local temporal signal. Green dots represent times during which the unit is in its spiking state; obviously, a discrete (integration) time is required to have a finite number of spikes per interval of local activity. C. Distribution of avalanche sizes for various subsampling trials, using the criterion sketched in B to define events. The black dotted line is the power law with exponent $3/2$ plotted as a guide to the eye.

Threshold effects. The standard empirical method to detect avalanches, as defined in (12), is intrinsically affected by some arbitrariness in parameter choices, that has been already discussed in the literature (12, 13). In particular, one arbitrary parameter is the threshold value θ above which the state "on" or "spiking" is declared [*] The common belief is that if, as a matter of fact, the system is scale-invariant, this value should not affect the large scale properties, such as exponent values. However, one has to be particularly careful with any thresholding procedure. For example, while for a standard one-dimensional random-walk process the avalanche exponents are independent of the threshold value chosen, this is not the case for other stochastic processes, e.g. birth-death processes (14). Moreover the threshold value should not be chosen too high relatively to the amplitude of the signal in order to avoid splitting an event into multiple (correlated) ones (15).

Recording a spike every time that the system crosses a very small threshold exposes the measurements to the effects of small fluctuations around the origin, induced by the multiplicative demographic noise term in Eq.1 in the main text (see Fig. 11). In order to avoid such a problem, it is possible to set also a second threshold value A_{min} for the minimal area for a spiking event to be considered as such; below such a threshold, activity is considered just a noise effect and, hence, disregarded. As illustrated in Figure 12 the statistics of avalanches does not depend significantly on the value chosen for such a threshold, A_{min}.

[*] In order to avoid spurious effects and consistently with the definition of avalanches as activity propagating marginally before falling into an absorbing state ($\rho = 0$), we choose a small value $\theta \ll 1$ (namely $\theta = 10^{-4}$).

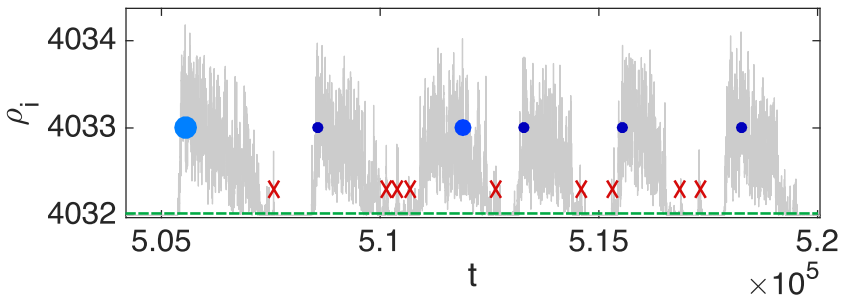


Fig. 11. Illustration of small events in the signal of the activity of one unit. Events covering a very small area (marked with red crosses) are neglected, while proper spikes are marked with blue full dots (smaller darker dots correspond to spikes with smaller area).

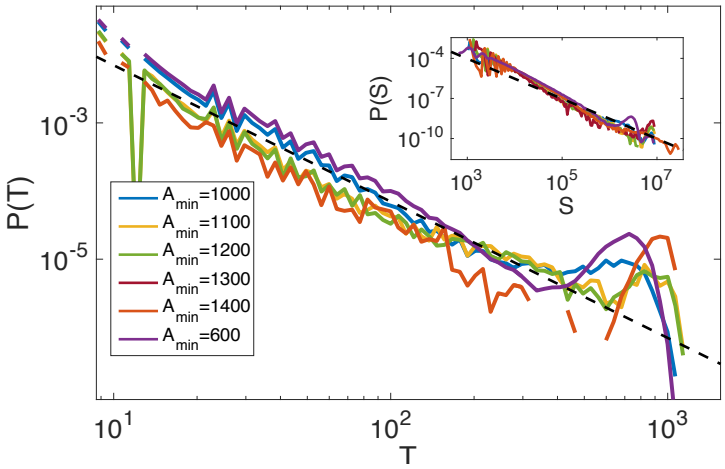


Fig. 12. Independence on the avalanche exponent values on the value chosen for the threshold on the minimal area A_{min}, used to declare "activity". Apart from the details of the substructure of the distribution, no qualitative dependence can be found by varying the value of A_{min}, both in avalanche-time (main plot) and avalanche-size (inset) distributions.

Experimentally inspired procedure to measure avalanches. Here, we briefly explain the steps necessary to perform a measure of an avalanche's size and duration, starting from a raster plot, as usually done in experimental setups (12). First of all, the Inter-Spike-Interval (ISI) is measured, as the average time interval between two consecutive spikes of (whichever 2 elements of) the network. Then the raster plot is divided in contiguous bins of width equal to the IEI (see Fig.5C in the main text). A bin is considered "empty" if no events are reported within it, and "occupied" otherwise. Consecutive series of occupied bins, preceded and ended by an empty one, define an avalanche. The avalanche duration is just the time interval between the preceding and the ending empty bins, and avalanche size is the total number of spikes that occurred in that time-interval. Since the individual signal in our analysis stems from a coarse grained section of neural tissue, we assign a weight to each event, representing the number of spikes within it, and determined by the integral of the signal during the event (see Fig.5A). Thus the only difference between the procedure we employ and the experimental one (12) is that the size of an avalanche is defined in our case as the *weighted* sum of the events during an avalanche.

System-size dependence. At the critical point of a phase transition, scale-invariant behavior is expected to be only limited by system size. This effect, which has been reported to be observed in experiments on neural avalanches (12), is also a hint in favor of true scale invariance, since finite size scaling holds when the system is at its critical point. In Figure 13 avalanche size and duration distributions are compared for various system sizes; as expected, larger systems show larger avalanches with progressively larger cut-off scales, while the overall size (resp. time) distribution keeps following a power law trend with the usual exponents $\tau = 3/2$ (resp. $\alpha = 2$; see inset).

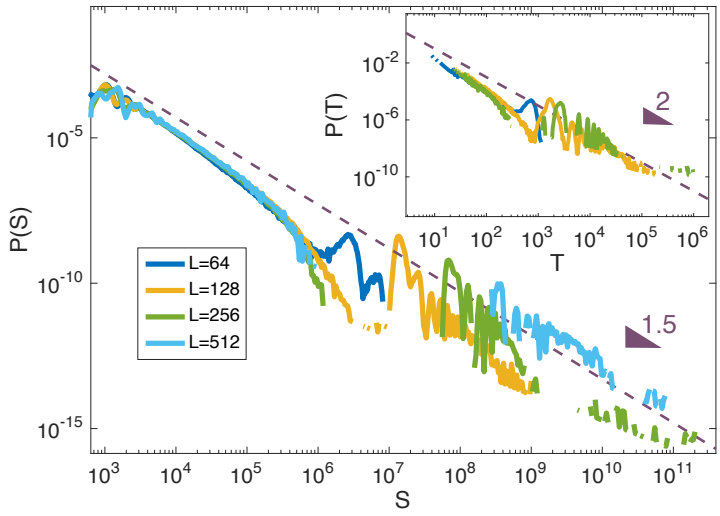


Fig. 13. Avalanche size S and duration T distributions for system sizes $N = 2^{12}, 2^{14}, 2^{16}, 2^{18}$. Although finite size scaling is not perfect, as the system size grows progressively larger, larger avalanches are found. Dashed lines represent an hypothetic power law trend with $\tau = 3/2$ and $\alpha = 2$.

SI7. Oscillations coexisting with scale invariance. Usually, scale-free avalanches of activity can be measured at the critical point of an *absorbing-state phase transition*. When the concept of "avalanche" is employed to describe the critical point of a synchronization phase transition, the marginal oscillatory nature of the system introduces a characteristic time scale in the synchronous phase –i.e. the period of the oscillations– which, in principle, is in contrast with the idea of scale-invariance. However, the two concepts can coexist –at least within certain limited scales– as illustrated in Figure 14. It shows that the structure (e.g. the peaks) in the avalanche-time distribution (inset) corresponds to the period of oscillation of a macroscopic variable (the total number of spikes, in the main plot); for instance, an isolated network synchronization event has a typical duration of 2000 (in arbitrary units), a sequence of two, about 5000, etc. On the other hand, the whole distribution, once these peaks are ignored can be approximately described as a power law with the expected exponent value.

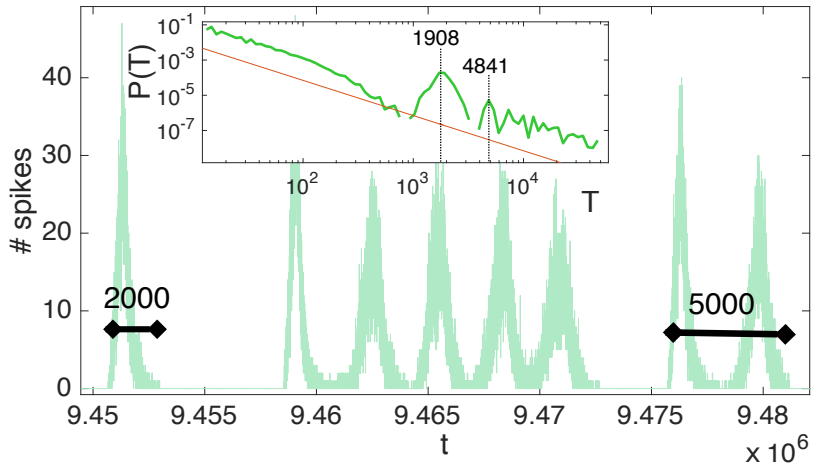


Fig. 14. Analysis of the structure underlying the avalanche-duration distributions. The main figure shows the total number of spikes at time t. Irregular oscillations of the global activity can be recognized, as the system is close to the edge of the synchronization phase transition. The characteristic period of an isolated oscillation corresponds to the peak in the avalanche duration distribution, while its multiples correspond to smaller peaks. System size $N = 128^2$.

REFERENCES

1. Wilson HR, Cowan JD (1972) Excitatory and inhibitory interactions in localized populations of model neurons. *Biophys. J.* 12(1):1–24.
2. Markram H, Tsodyks M (1996) Redistribution of synaptic efficacy between pyramidal neurons. *Nature* 382:807–810.
3. Benayoun M, Cowan JD, van Drongelen W, Wallace E (2010) Avalanches in a stochastic model of spiking neurons. *PLoS Comput. Biol.* 6(7):e1000846.
4. Sporns O (2010) *Networks of the Brain.* (MIT Press, USA).
5. Jbabdi S, Sotiropoulos SN, Haber SN, Van Essen DC, Behrens TE (2015) Measuring macroscopic brain connections in vivo. *Nat Neurosci* 18(11):1546–1555.
6. Watts DJ, Strogatz SH (1998) Collective dynamics of small-world networks. *Nature* 393(6684):440–442.
7. Okujeni S, Kandler S, Egert U (2017) Mesoscale architecture shapes initiation and richness of spontaneous network activity. *J. Neurosci.* 37(14):3972–3987.
8. Mantegna RN, Stanley HE (1999) *Introduction to econophysics: correlations and complexity in finance.* (Cambridge university press).
9. Peng C, Havlin S, Stanley HE, Goldberger AL (1995) Quantification of scaling exponents and crossover phenomena in nonstationary heartbeat time series. *Chaos: An Interdisciplinary Journal of Nonlinear Science* 5(1):82–87.
10. Hu K, Ivanov PC, Chen Z, Carpena P, Stanley HE (2001) Effect of trends on detrended fluctuation analysis. *Phys. Rev. E* 64(1):011114.
11. Linkenkaer-Hansen K, Nikouline VV, Palva JM, Ilmoniemi RJ (2001) Long-range temporal correlations and scaling behavior in human brain oscillations. *Journal of Neuroscience* 21(4):1370–1377.
12. Beggs JM, Plenz D (2003) Neuronal avalanches in neocortical circuits. *J. of Neurosci.* 23(35):11167–11177.
13. Petermann T, et al. (2009) Spontaneous cortical activity in awake monkeys composed of neuronal avalanches. *Proc. Natl. Acad. Sci. USA* 106(37):15921–15926.
14. Font-Clos F, Pruessner G, Moloney NR, Deluca A (2015) The perils of thresholding. *New J. Phys.* 17(4):043066.
15. Laurson L, Illa X, Alava MJ (2009) The effect of thresholding on temporal avalanche statistics. *J. Stat. Mech. Theory E* 2009(01):P01019.